J. Print Media Technol. Res. – Vol. 13 No. 3 (2024)
February 2025

3-2024

ISSN 2414-6250 (Online)
UDC 665

Journal of Print and Media Technology Research

Scientific contributions

ISSN 2414-6250

Editor-in-Chief
Daniel Bohn (Wuppertal)

Published by iarigai
www.iarigai.org

The International Association of Research Organizations for the Information, Media and Graphic Arts Industries

J. Print Media Technol. Res. – Vol. 13 No. 3 (2024)
February 2025
ISSN 2414-6250 (Online)
A print version is available on-demand
ISSN 2223-8905 (Print)

Journal of Print and Media Technology Research

A PEER-REVIEWED QUARTERLY

PUBLISHED BY

The International Association of Research Organizations
for the Information, Media and Graphic Arts Industries
Magdalenenstrasse 2, D-64288 Darmstadt, Germany
http://www.iarigai.org
journal@iarigai.org

A mission statement

To meet the need for a high quality scientific publishing platform in its field, the International Association of Research Organizations for the Information, Media and Graphic Arts Industries is publishing a quarterly peer-reviewed research journal.

The journal is fostering multidisciplinary research and scholarly discussion on scientific and technical issues in the field of graphic arts and media communication, thereby advancing scientific research, knowledge creation, and industry development. Its aim is to be the leading international scientific journal in the field, offering publishing opportunities and serving as a forum for knowledge exchange between all those interested in contributing to or learning from research in this field.

By regularly publishing peer-reviewed, high quality research articles, position papers, surveys, and case studies as well as review articles and topical communications, the journal is promoting original research, international collaboration, and the exchange of ideas and know-how. It also provides a multidisciplinary discussion on research issues within the field and on the effects of new scientific and technical developments on society, industry, and the individual. Thus, it intends to serve the entire research community as well as the global graphic arts and media industry.

The journal is covering fundamental and applied aspects of at least, but not limited to, the following topics:

Printing technology and related processes

- Conventional and special printing
- Packaging
- Fuel cells and other printed functionality
- Printing on biomaterials
- Textile and fabric printing
- Printed decorations
- Materials science
- Process control

Premedia technology and processes

- Colour reproduction and colour management
- Image and reproduction quality
- Image carriers (physical and virtual)
- Workflow and management

Emerging media and future trends

- Media industry developments
- Developing media communications value systems
- Online and mobile media development
- Cross-media publishing

Social impact

- Media in a sustainable society
- Environmental issues and sustainability
- Consumer perception and media use
- Social trends and their impact on media

Submissions to the Journal

Submissions are invited at any time and, if meeting the criteria for publication, will be rapidly submitted to peer-review and carefully evaluated, selected and edited. Once accepted and edited, the papers will be published as soon as possible.

✉ Contact the Editorial office: journal@iarigai.org

Journal of Print and Media Technology Research

3-2024

February 2025

J. Print Media Technol. Res. – Vol. 13 No. 3 (2024), 121–174

Journal of Print and Media Technology Research is listed in:

Emerging Sources Citation Index

Scopus

DOAJ – Directory of Open Access Journals

Index Copernicus International

NSD – Norwegian Register for Scientific Journals, Series and Publishers

Printed in Germany

Contents

A letter from the Editor

Daniel Bohn
Editor-in-Chief
E-mail: danielbohn@jpmtr.org
journal@iarigai.org

Dear Readers,

It is my pleasure to introduce the latest issue of the Journal of Print and Media Technology Research. As always, our goal is to present research that advances knowledge in the print and media technology domain, highlighting both theoretical insights and practical applications. The selection of articles in this issue is a good example of the continued innovation in our common industry.

In this edition, we feature three research contributions.

The first paper, by Rafikov, et al., examines the microstructure, morphology, and properties of printing paper laminated with polypropylene film. Their study explores how an ethylene–vinyl acetate (EVA) copolymer adhesive solution enhances adhesion, overcoming the challenges typically posed by glossy paper surfaces. Through FT-IR spectroscopic and SEM-EDS analysis, the authors provide evidence that micropore penetration significantly strengthens laminated structures, offering a valuable contribution to the field of packaging and print durability.

The second paper, by Dimić-Mišić, et al., delves into the interaction of natural plant dye inks, rich in anthocyanins, with calcium carbonate containing substrates. As the demand for sustainable and plant-based inks grows, understanding how these dyes interact with alkaline substrates becomes increasingly important. This study presents an analysis of color shifts, refractive index variations, and strategies for improving ink–substrate compatibility. With implications for packaging, textiles, and specialty printing, this research highlights the need for further development of natural dye technologies to meet industrial performance requirements.

Finally, Brandenburg's research on the retroactive effect of variable tensile forces on lateral web motion and registration errors provides (again) fascinating insights into the stability of web-fed printing systems. By modeling the complex dynamics of transverse and longitudinal register errors, his study enhances our understanding of how tensile forces influence precision in continuous printing processes. These findings are particularly relevant for high-speed production environments where alignment accuracy is paramount.

Alongside these scientific contributions, our Topicalities section, curated by Markéta Držková, provides an overview of key industry developments. This issue highlights newly established and revised ISO standards in graphic technology, covering advancements in color reproduction, press calibration methods, and safety requirements for printing equipment. Additionally, this section reflects on insights from recent international conferences and technical forums, where automation, sustainability, and digital transformation in printing are the main topics.

In addition to these updates, we present highlights from recent doctoral dissertations, which further illustrate emerging research directions and technological

advancements. Antti Väisänen from the University of Eastern Finland explores chemical and particulate emissions in polymer-based 3D printing, shedding light on environmental and occupational safety challenges. Xinran Zhou, from Nanyang Technological University, develops 3D-printed piezoelectric energy harvesters with innovative kirigami and auxetic structures, advancing sustainable energy solutions for wearable electronics. Felix Braig of TU Darmstadt investigates solvent evaporation in printed liquid films using digital holographic interferometry, providing valuable insights for improving drying efficiency and print quality.

The Bookshelf section in this issue also introduces several noteworthy publications. Among them, *Motion and Path Planning for Additive Manufacturing* by Roschli, et al., offers practical insights into toolpath generation and advanced slicing techniques for additive manufacturing. Additionally, Laura S. Scherling's edited volume *Digital Transformation in Design Processes and Practices* explores the impact of digitalization on design workflows, presenting case studies on AI integration, digital typography, and evolving approaches to design education.

As we look ahead, the role of print media continues to evolve in response to technological advancements and shifting environmental priorities. The research featured in this issue not only contributes to academic discourse but also offers practical solutions to challenges faced by industry professionals. We remain committed to fostering collaboration between researchers and practitioners, ensuring that the journal serves as a bridge between innovation and application.

Wuppertal, February 2025

JPMTR-2405
DOI 10.14622/JPMTR-2405
UDC 678.5:678.742.5:678.742:678.7+539.23+543.42

Original scientific paper | 193
Received: 2024-02-24
Accepted: 2024-06-20

Microstructure, morphology and properties of printing paper laminated with polypropylene film

Adham Salimovich Rafikov[1], *Fazliddin Muhiddinovich Turaev*[2], *Anvar Abdugafarovich Djalilov*[2] *and Bekzod Shuxrat Ugli Ibodulloyev*[1]

[1]Tashkent Institute of Textile and Light Industry, asrafikov@mail.ru
Department of Chemistry, fazliddin5576@gmail.com
Shakhdjakhon Street 5, 100100, Tashkent, Uzbekistan anvar-matbaa@mail.ru
[2]Tashkent Institute of Textile and Light Industry, bshibodulloyev@mail.ru
Department of Technology of Printing and Packing Industry,
Shakhdjakhon Street 5, 100100, Tashkent, Uzbekistan

Abstract

To improve design, reduce wear, and extend service life, lamination involves applying a thin polymer film to paper or cardboard using hot melt adhesive or a solution. Moreover, hot melt adhesive bonds well to a fairly rough or matte surface. If the surface of the paper or cardboard is smooth or glossy, then molten high molecular weight polymer adhesive does not always penetrate its micropores. Due to differences in melting temperatures between the polymer adhesive and the polymer film, the polymer adhesive does not bond strongly enough to the polymer film. In this study, in order to increase the adhesive strength between paper and polymer film, glossy paper was laminated with polypropylene film using an adhesive solution of ethylene–vinyl acetate (EVA) copolymer. A polymer adhesive solution, unlike a melt, penetrates into the micropores of glossy paper and ensures strong adhesion of the polymer film to the paper surface. FT–IR spectroscopic studies of polypropylene, EVA copolymer, and laminated paper showed the absence of chemical interaction between them during the lamination process. As studies on SEM-EDS analysis have shown, the adhesion interaction between the polymer film and the adhesive occurs due to ethylene units, and between the paper and adhesive due to vinyl acetate units. In contrast to the industrial sample with hot melt adhesive, in the experimental paper sample, near the polypropylene film, micropores are filled with a polymer adhesive solution. Elemental analysis of torn layers of laminated paper shows the presence of polymer adhesive in the micropores of the paper layer. The adhesive strength between layers of laminated paper is 20 % higher, and the penetration force is 40 % greater than that of the industrial sample.

Keywords: laminate, paper and cardboard, polypropylene, ethylene–vinyl acetate copolymer, adhesion.

1. Introduction

Polymers in the form of a carrier of text and illustration information, protective film and layered materials, and adhesives are widely used in printing (Radermacher, 2016; Gregor-Svetec, 2022) and in packaging production (Riley, 2012). Large-scale industrial polyolefins, such as polyethylene and polypropylene, as well as their copolymers and derivatives (Posch, 2011), have long been used for laminating paper and cardboard. Lamination printing is the process of applying a thin polymer film to paper or other comparable substrates to enhance and protect a printed layer. It is used for covers of books, magazines, brochures, business cards and other printed products. Lamination is also used to produce various types of packaging materials and paper for insulating electrical cables (Furuse and Fuchino, 2014). Lamination refers to a printing finishing process in which a thin layer of plastic laminate is bonded to the surface of paper or cardboard using pressure and heat. Lamination has the following goals: improving design and appearance, increasing strength and other physical and mechanical properties, reducing wear and increasing the service life of printed products.

Laminates are typically applied to the front surface of book and magazine covers, but can be applied to both sides of the printed product. Laminate can have dif-

ferent thicknesses and degrees of gloss. Commercial printers use a combination of heat, pressure, tension and an adhesive to apply the laminated film.

The composition of the lamination film contains two main components: a polymer film and an adhesive layer. Polyethylene terephthalate (PET) (Charinee, et al., 2021), polybutylene terephthalate (PBT) (Repeta, et al., 2020), polyethylene (PE) (Galikhanov and Musina, 2012; Kibirkštis, et al., 2022), polypropylene (PP) (Furuse and Fuchino, 2014; Rousseau, et al., 2023) and polyvinyl chloride (PVC) (Pilipović, 2022) are often used as polymer films. Ethylene vinyl acetate copolymer (EVA) (Shih and Hamed, 1997; Paul, 2023; Li, et al., 2008; Moyano, et al., 2008; Rafikov, et al., 2022), polyurethane adhesive (Yan, et al., 2020; Stiene, et al., 2019), epoxy adhesive (Sharma, et al., 2023) or other adhesive material are used as the adhesive layer. The quality of the laminate depends on both the thickness and the ratio of components (Repeta, et al., 2018). The thickness of the polymer film for lamination ranges typically from 8 to 250 μm, which depends on the scope of application or the product. The polymer adhesive is attached to a polymer film either from a melt by hot extrusion or from a solution by spraying or rolling.

Lamination film with an adhesive layer can be applied to the surface of paper or cardboard using a hot or cold method (Prambauer, et al., 2016). In the first case, the treated surface, like the film itself, is heated to at least 70 °C. This causes the adhesive layer to melt, allowing it to bond with the sheet of the printed products. This method of applying a laminate coating is the most common. Most commercially available films are designed for hot application. Applying a PP film to a substrate using the hot method reduces processing time and pressure (Peng, et al., 2020). Cold-apply film is used for laminating documents and other papers, such as valuable archival records, for which exposure to high temperatures can be detrimental. In this case, the surface to be treated is covered with the lamination film and passed through a special press. Under the influence of high pressure, the adhesive applied to the layer of polymer film softens and the film adheres to the surface of the document.

In recent years, manufacturers have been inclined to use PP film for laminating book and magazine covers, which is more transparent than PE and PVC. Also, it is more elastic and cheaper than PET. As an adhesive polymer, preference is often given to EVA copolymer. The EVA copolymer shows a good adhesion to surfaces of non-polar polyolefin films due to ethylene units, and to the surface of paper due to vinyl acetate units. Printing enterprises of the Republic of Uzbekistan use PP laminating film with a layer of hot melt adhesive EVA copolymer made in China. This laminate is applied to the surface of paper and cardboard by hot pressing. During thermal exposure, PP and the EVA copolymer are in a highly elastic, almost liquid state, while paper, as an infusible material, remains in a solid state. If the paper is sufficiently porous, then the molten polymer adhesive penetrates into these pores and binds well to the paper. This lamination film does not have sufficiently high adhesion to the surface of smooth or glossy paper, since the high molecular weight polymer does not penetrate into the micropores of the paper. In this case, the adhesive solution has an advantage; a low-molecular solvent easily and quickly penetrates the micropores of paper, drawing the polymer along with it. The purpose of this study is to increase the adhesive strength between polymer film and paper by using an adhesive solution of EVA copolymer.

2. Materials and methods

2.1 Materials

Glossy paper with a grammage of 220 g/m^2 was selected for lamination tests. The laminating film used was a biaxially oriented polypropylene (PP) film with a thickness of 20 μm. For gluing PP film to paper, the colorless copolymer polyethylene vinyl acetate (PEVA) was chosen as granules. Xylene with toluene impurities (technical grade) was used as a solvent. As an analogue, we selected industrial PP film with an adhesive layer for laminating paper with a thickness of 24 μm.

2.2 Method for producing laminated paper

2.2.1 Preparation of PEVA adhesive solution

Several PEVA granules were placed in a glass with a lid, the calculated amount of solvent (1 g EVA, 10.46 g solvent) was poured on top, the lid was closed, and left for a day to swell. The contents were then vigorously stirred, slightly heated (70 °C) in a hot water bath until a homogeneous viscous solution was formed. Solutions with different concentrations of PEVA were obtained by diluting the original solution.

2.2.2 Applying adhesive to the surface of the PP film

Work with PP film was carried out using surgical gloves to prevent contamination of the surface of the film. A 0.1 mm thick adhesive solution was applied to the inner surface of the PP film using a squeegee device. The adhesive layer is dried under a fume hood at room temperature for 2–3 minutes.

2.2.3 Paper lamination

The lamination process was carried using an "A4 Exact LR-H001" installation by tanning layers of paper and PP film with PEVA adhesive under pressure from rollers

at a temperature of 90–100°C. The width of the rollers was 20 cm. The diameter of the rollers was 3 cm and the speed of paper passing was 0.66 ± 0.04 m/min.

2.3 Testing the properties of laminated paper

The structure of the samples was analyzed using Fourier Transform Infrared Spectroscopy (FT-IR) with a Nicolet IN10 spectrometer from Thermo Fisher Scientific (USA), covering a scanning range of 500–4000 cm^{-1}.

The surface morphology and elemental composition of the samples were analyzed using a scanning electron microscope (JSM-IT200LA InTouchScope, Japan) equipped with an energy-dispersive spectroscopy (SEM-EDS) application.

The adhesive strength between the polymer film and paper was determined by the peel force (N) of the film using a Shimadzu AGS-X device. A sample of laminated paper measuring 10 × 5 cm was adhesived to the clamps of the device and the force required to completely tear off the film from the surface of the paper was determined.

The bending resistance of the paper was measured using an endurance testing machine (HD-A519-2) from Haida Equipment Co., Ltd. For this test, a strip measuring 150 x 12 mm was cut from a sample of laminated paper. The device was used to determine the number of double bends required to completely destroy the sample.

The resistance of the paper to piercing was determined using a bursting strength testing machine (HD-A504-2) from Haida Equipment CO., LTD. for a sample size of 130 × 100 mm.

3. Results and discussion

3.1 FT-IR spectra

Fourier transform infrared spectroscopic studies were carried out to clarify the nature of the interaction of PP film, PEVA adhesive and paper with each other. The obtained FT-IR spectra are presented in Figure 1.

The FT-IR spectra of the PP film show absorption bands characteristic for stretching (ν) and bending (δ) vibrations of C–H and C–C bonds: in the regions of 2949–2839 cm^{-1} for $\nu_{(C-H)}$; in the regions of 1456–1304 cm^{-1} and 528–459 cm^{-1} for $\delta_{(C-H)}$; and in the regions of 1359 – 809 cm^{-1} for $\nu_{(C-C)} + \delta_{(C-C)}$.

The FT-IR spectra of PEVA adhesive revealed absorption bands characteristic for stretching and bending vibra-

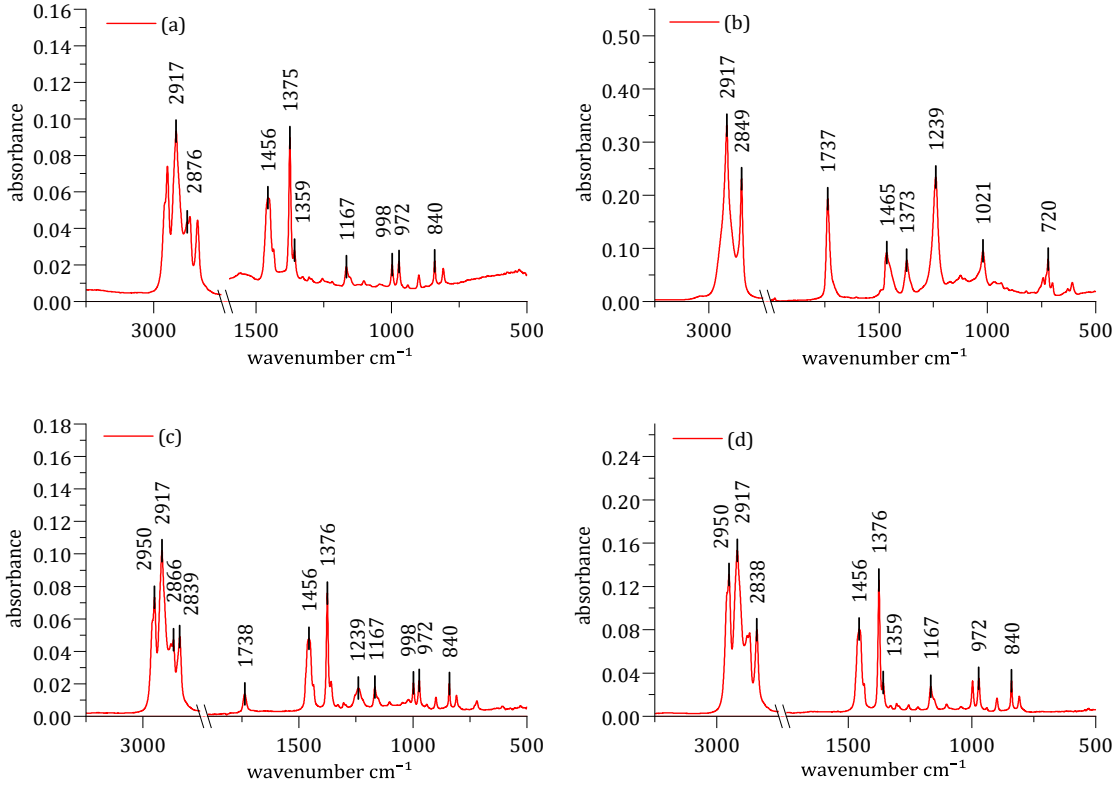

Figure 1: FT-IR spectra of PP (A), PEVA (B), PP-PEVA laminating film (C) and laminated paper (D)

tions of PEVA bonds: at 2917 and 2849 cm^{-1} for $\nu_{(C\text{-}H)}$; at 1737 cm^{-1} – $\nu_{(C=O)}$; at 1465, 1372 and 743–608 cm^{-1} for $\delta_{(C\text{-}H)}$; in the region of 1239–821 cm^{-1} for $\nu_{(C\text{-}O)} + \nu_{(C\text{-}C)} + \delta_{(C\text{-}O)}$.

In the FT-IR spectra of the PP film with PEVA adhesives, absorption bands of polypropylene and PEVA bonds were detected, including $\nu_{(C=O)}$ at 1738 cm^{-1}, but with lower intensity than in the adhesive itself.

In the FT-IR spectra of laminated paper, the previously observed absorption bands are retained, along with additional bands characteristic of cellulose, such as a low-intensity broad band $\nu_{(O\text{-}H)}$ at 3282 cm^{-1}.

The absence of obvious new absorption bands in the combined products indicates that during the lamination process there is no chemical interaction between the components, but an adhesive interaction.

3.2 SEM-EDS analysis

The SEM-EDS analyses were carried out to determine the surface morphology and cross-section of samples of PP film with PEVA adhesive, laminated paper, as well as to determine the nature of the interaction of the adhesive with paper and polymer film. Figure 2 shows a cross-section of a PP film with an adhesive layer. As can be seen from Figure 2, the industrial laminating film consists of three layers with a total thickness of 20–23 μm; the thickness of the adhesive layer is 6–10 μm. The laminating film prepared in this study consists of two layers with a total thickness of 26–29 μm; the thickness of the adhesive layer is 8–12 μm.

Figure 3 shows the fibrous-porous structure of the paper and the layer of polymer film on its surface. The thickness of the laminated paper together with the polymer film was 210–220 μm. In contrast to the industrial sample, the micropores of the experimental paper (near the PP film) are filled with a polymer adhesive solution. Apparently, the polymer adhesive solution seeps into the interfiber space of the paper, and at the same time partially dissolves the contact surface of the PP film. All this should lead to increased adhesive interaction between the surface of the paper and the laminating film. To confirm this, SEM-EDS analysis of each layer of laminated experimental paper was carried out (Figure 4). It can be seen that the energy dispersive spectra were taken from three scanned areas of the laminated paper. The first region refers to the cross section

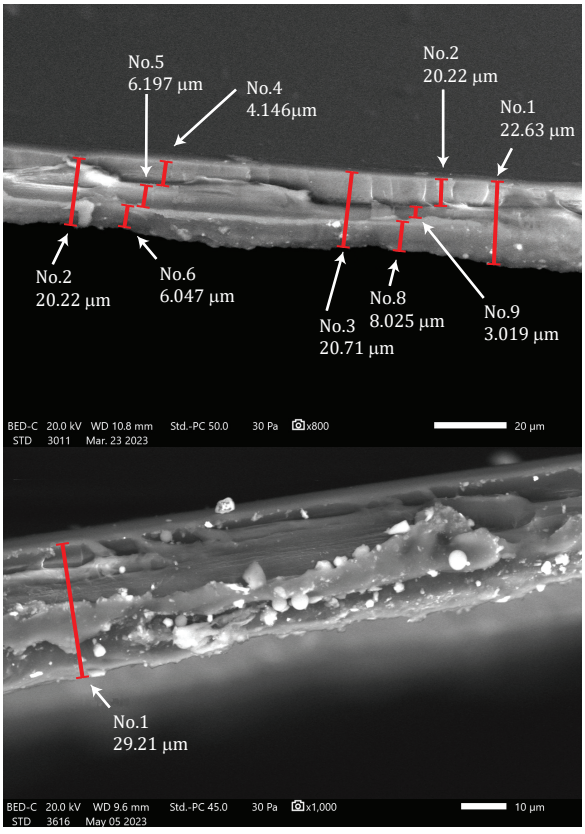

Figure 2: SEM image of the cross section of a PP – laminating film: (top) – industrial sample, (bottom) – experimental sample

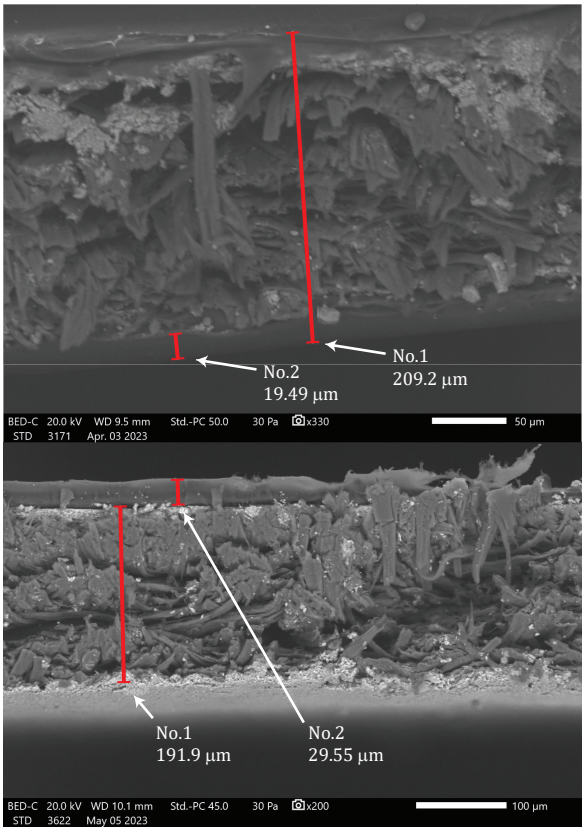

Figure 3: SEM images of a cross section of paper laminated with commercial (top) and experimental (bottom) PP film

of the PP film, where carbon atoms should be detected. It turned out that there is also oxygen in this area. Apparently, oxygen belongs to the PEVA, which confirms the previously stated assumption that some of it passes into the PP film as a result of partial dissolution. The second region contains carbon and oxygen atoms, in a ratio that approximately corresponds to PEVA. This confirms another assumption about the transition of the adhesive solution into the micropores of the paper. The mass ratio of carbon and oxygen in the third region corresponds to the composition of paper pulp.

SEM-EDS studies continued at the interface between paper and polymer film (Figure 6). The observed picture of the surface of the polymer film after forceful tearing under load provided information about the relationship between the forces of adhesion and cohesion in laminated paper. Traces of paper in the form of white spots are visible on the film interface. The elemental composition of the three areas of these stains is approximately the same, and corresponds to the composition of mineral-filled paper. Judging by the presence of large amounts of calcium, the filler is calcium carbonate or chalk. These stains are an agglomerate of chalk particles with cellulose fibers. The elemental composition of four more surface areas where there are no white spots was scanned. In these areas, carbon and oxygen atoms of approximately the same composition were found, which corresponds to the composition of PEVA. The results indicate that the adhesion forces of PEVA adhesive with PP film are much stronger than with paper; when torn, the adhesive almost completely transfers to the surface

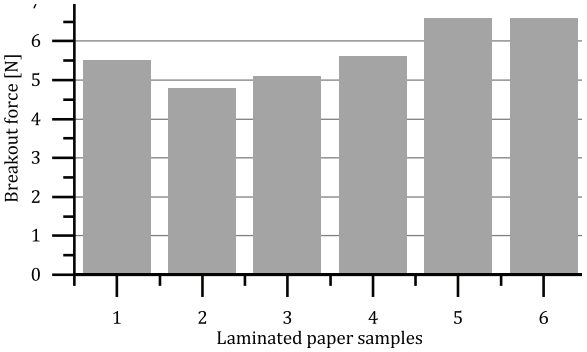

Figure 5: Breaking force of PP film from the paper surface: industrial analogue (1); experimental samples using PEVA adhesive solution with concentrations of 8 % (2), 9 % (3), 10 % (4), 11 % (5) and 12 % (6)

of the film. The adhesive forces of interaction between PEVA and the surface of the paper are comparable to the cohesive forces inside the paper. Moreover, a piece of paper comes off at the weakest link – in places where mineral filler accumulates.

3.3 Physical-mechanical properties

The following studies were carried out to determine the adhesive interaction forces between layers in comparison with the industrial analogue. Figure 5 shows the dependence of the breaking force between PP film and paper on the type of laminated paper and the concentration of PEVA adhesive solution. As can be seen from Figure 6, an increase in the concentration of PEVA

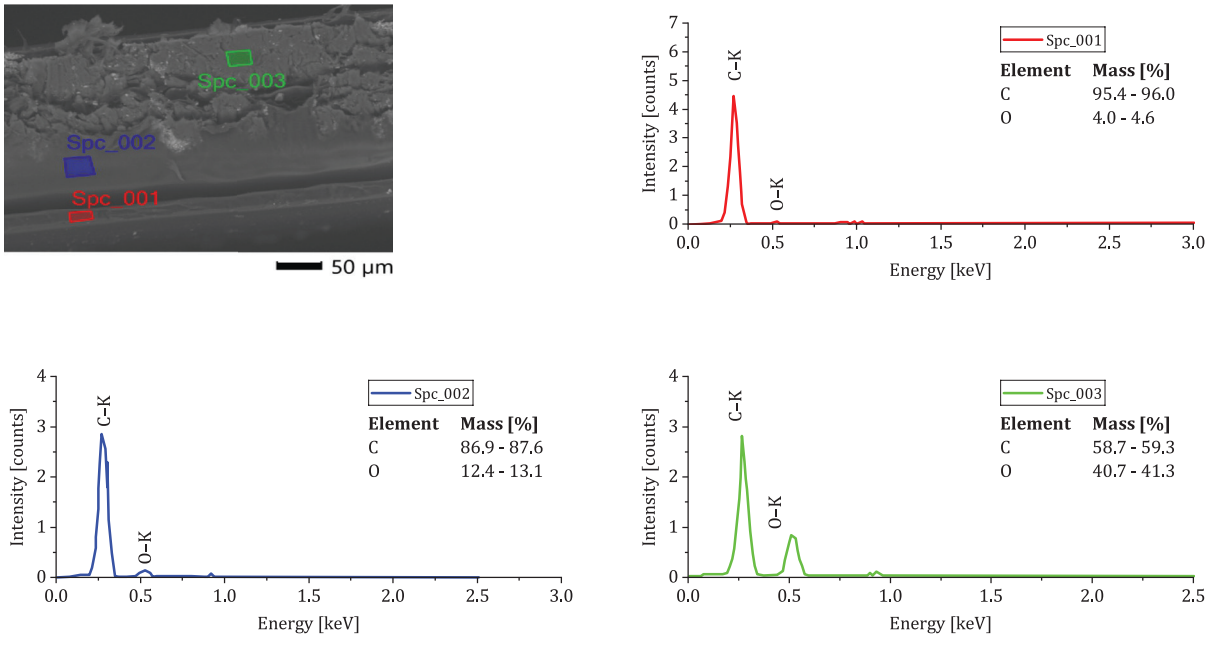

Figure 4: SEM-EDS analysis of layers of experimental laminated paper

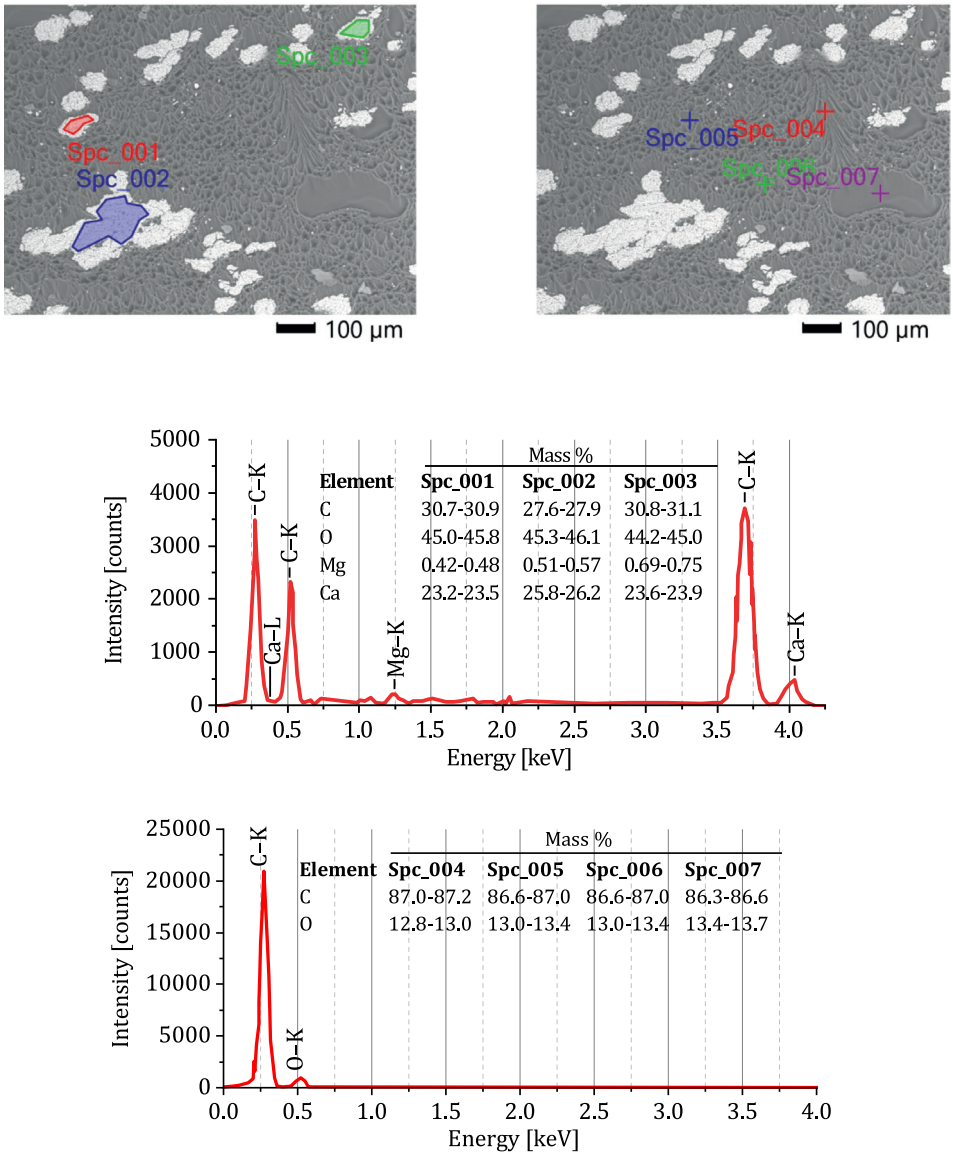

Figure 6: SEM-EDS analysis of the interface between PP film and paper of an experimental sample of laminated paper

solution to 11 %, the adhesive strength between the polymer film and paper increased. Moreover, the adhesion strength of the film in this sample was approximately 20 % higher than in the sample of the industrial analogue. These data confirm the assumption that the adhesive solution penetrated into the micropores of the paper. For a sample obtained using an 11 % solution of PEVA adhesive, some other important indicators of laminated paper were determined (Table 1).

As can be seen from Table 1, at the same grammage, the analogue and the experimental sample can withstand more than 100 double bends. The bursting pressure of the experimental sample is 1.4 times higher than that

Table 1: Physical-mechanical properties of laminated paper

Sample	Grammage [g/m²]	Bending resistance, number of double bends	Pressure resistance [kPa × m²/g]
Paper without lamination	220 ± 3	15	–
Industrial Aanalоge	240 ± 4	more than 100	3.68 ± 0.06
Laminated paper	245 ± 4	more than 100	5.12 ± 0.06

of the analogue. The data obtained shows the obvious advantages of laminating glossy paper with PP film using a PEVA adhesive solution.

4. Conclusion

Bonding smooth or glossy paper and cardboard to polypropylene film using an ethylene-vinyl acetate copolymer adhesive solution has significant advantages over gluing using hot melt adhesive. Due to the stronger adhesive interaction of the adhesive solution with both the surface of the paper and the surface of the polymer film. The solvent partially dissolves the polypropylene, which ensures strong adhesion of the film to the adhesive. At the same time, the solvent, together with the adhesive macromolecule, penetrates into the micropores of the paper, which ensures strong adhesion of the paper to the adhesive. Additionally, stronger adhesive interaction between the layers provides, in turn, better overall physical and chemical mechanical properties of the laminate. A direct comparison of the properties of an industrial paper–polypropylene laminate produced using hot melt adhesive and an experimental laminate with the same grammage showed the following: the force for tearing off layers, the number of double bends and the force for punching the experimental laminate are approximately consistently 20 – 40% higher than the industrial analogue.

References

Charinee, W., Ajcharaporn, A., Jintapatee, I., Boonsita, P., Witchuda, D., 2021. Laser perforation of polyethylene terephthalate / polyethylene laminated film for fresh produce packaging application. *Food Packaging and Shelf Life*, 28: 100677. https://doi.org/10.1016/j.fpsl.2021.100677.

Furuse, M. and Fuchino, S., 2014. Analysis and measurement of thermal conductivity of polypropylene laminated paper impregnated with subcooled liquid nitrogen. *Cryogenics*, 63, pp. 125–128. https://doi.org/10.1016/j.cryogenics.2014.02.021.

Galikhanov, M.F. and Musina, L.R., 2012. Changes in the physical and mechanical properties of corrugated cardboard when it is coated with polyethylene. *Forest Journal*, 5, pp. 143–148.

Gregor-Svetec, D., 2022. Chapter 14 – Polymers in printing filaments. In: Polymers for 3D Printing. *J. Izdebska-Podsiadły*, ed. Plastics Design Library, William Andrew Publishing, pp.155–269. https://doi.org/10.1016/B978-0-12-818311-3.00002-1.

Kibirkštis, E., Mayik, V., Zatserkovna, R., Vaitasius, K., Stepanenko, A., Kandrotaitė-Janutienė, R., Venytė, I. and Danilovas, P.P., 2022. Study of physical and mechanical properties of partially biodegradable LDPE polymeric films and their application for printing and packaging. *Polymer Testing*, 112: 107646. https://doi.org/10.1016/j.polymertesting.2022.107646.

Li, W., Bouzidi, L., Narine, S.S., 2008. Current research and development status and prospect of hot-melt adhesives: A review. *Industrial & Engineering Chemistry Research*, 47, pp. 7524–7532. https://doi.org/10.1021/ie800189b.

Moyano, M.A., Paris, R., Martin-Martinez, J.M., 2008. Viscoelastic and adhesion properties of hot-melts made with blends of ethylene-co-n-butyl acrylate (EBA) and ethylene-co-vinyl acetate (EVA) copolymers. *International Journal of Adhesion and Adhesives*, 88, pp. 34–42. https://doi.org/10.1016/j.ijadhadh.2018.11.001

Paul, C.W., 2023. Hot-melt adhesives. *MRS Bulletin*, 28, pp. 440–444. https://doi.org/10.1557/mrs2003.125.

Peng, X., Liu, X., Huang, Y., Sang and L., 2020. Investigation of joining of continuous glass fibre reinforced polypropylene laminates via fusion bonding and hotmelt adhesive film. *International Journal of Adhesion and Adhesives*, 100: 102615. https://doi.org/10.1016/j.ijadhadh.2020.102615.

Prambauer, M., Paulik, Ch. and Burgstaller, Ch., 2016. Evaluation of the interfacial properties of polypropylene composite laminates, reinforced with paper sheets. *Composites Part A: Applied Science and Manufacturing*, 88, pp. 59–66. https://doi.org/10.1016/j.compositesa.2016.05.016.

Posch, W., 2011. *3* – Polyolefins. In: Applied Plastics Engineering Handbook, *M. Kutz*, ed., William Andrew Publishing, pp. 23–48. https://doi.org/10.1016/B978-1-4377-3514-7.10003-0.

Radermacher, K., 2016. Environmental and safety issues of polymers and polymeric material in the printing industry. In: Printing on Polymers, *J. Izdebska and S. Thomas*, eds., William Andrew Publishing, pp. 397–415. https://doi.org/10.1016/B978-0-323-37468-2.00025-7.

Rafikov, A., Mirzayev, N. and Alimkhanova, S., 2022. Multilayer nonwoven lining materials made of wool and cotton for clothing and footwear. *Journal of Industrial Textiles*, 51(4), pp. 6172–6194. https://doi.org/10.1177/15280837211060881.

Repeta, V., Kukura, Y., Shibanov, V., Myklushka, I. and Kukura, V., 2020. Influence of properties of materials for solventless lamination on the bonding strength of multilayer packaging. *Journal of Print and Media Technology Research*, 9(3), pp. 177–184. https://doi.org/10.14622/JPMTR-2001.

Repeta, V., Kukura, Y. and Kukura, V., 2018. Analysis of the relationship of quality factors in the solventless lamination process. *Journal of Print and Media Technology Research*, 7(1), pp. 27–34. https://doi.org/10.14622/JPMTR-1806.

Riley, A., 2012. Basics of polymer chemistry for packaging materials, In: *Packaging Technology: Fundamentals, Materials and Processes*. Cambridge: Woodhead Publishing, pp. 262–286. https://doi.org/10.1533/9780857095701.2.262.

Rousseau, J., Donkeng, N.E.N., Farcas, F., Chevalier, S. and Placet, V., 2023. Thermal and hydrothermal ageing of flax / polypropylene composites and their stainless steel hybrid laminates. *Composites Part A: Applied Science and Manufacturing*, 171: 107582. https://doi.org/10.1016/j.compositesa.2023.107582.

Sharma, P., Yadav, A., Meena, M., Roy, P. and Nebhani, L., 2023. Epoxy-based reflective adhesive for lamination of single-sided metallized film over glass fabric destined for its use as reflective layer in fire proximity clothing. *Polymer Degradation and Stability*, 213: 110365. https://doi.org/10.1016/j.polymdegradstab.2023.110365.

Shih, H.H. and Hamed G.R., 1997. Poly(ethylene-co-vinylacetate) based hot melt adhesives: I. Relating adhesive rheology to peel adhesion. *Journal of Adhesion*, 61, pp. 23–245. https://doi.org/10.1080/00218469708010524.

Stiene, T., Urban, P. and Rodriguez-Giles, J.M., 2019. Prediction of lamination-induced colour shifts for UV offset printings by using a heuristic approach as well as machine learning techniques. *Journal of Print and Media Technology Research*, 8(4), pp. 199–207. https://doi.org/10.14622/JPMTR-1912.

Yan, J.W., Hu, C., Tong, L.H., Lei, Z.X., and Lin, Q.B., 2020. Migration test and safety assessment of polyurethane adhesives used for food-contact laminated films. *Food Packaging and Shelf Life*, 28: 100449. https://doi.org/10.1016/j.fpsl.2019.100449.

JPMTR-2410
DOI 10.14622/JPMTR-2410
UDC 519.6:621.798:658.5:677.027

Scientific paper | 194
Received: 2024-01-17
Accepted: 2024-12-02

Retroactive effect of variable tensile forces on lateral web motion and lateral registration errors

Günther Brandenburg

Tölzer Str. 41, 82194, Gröbenzell, Germany gap.brandenburg@t-online.de

Abstract

The lateral position of a continuous web can be determined by a control roller at an angle to the longitudinal direction of web motion together with subsequent auxiliary rollers. However, a change in the tensile force changes this lateral position. The solution of the system of descriptive differential equations leads to a separate treatment of pure translation and pure rotation of the control roller. However, a resulting block plan for the dynamics of lateral motion was found, which is combined with the longitudinal mass flow and the retroactive effect of variable tensile forces on the lateral motion. Transverse and longitudinal register errors in the multi-roller system can be mapped together with the mass flow chain in the form of a multi-layer model. This enables extensive simulations of all system quantities as well as the design and optimization of control loops.

Keywords: lateral web motion, longitudinal mass flow chain, lateral and longitudinal register errors, variable tensile forces, retroactive effect, multi-layer model

1. Introduction

The subject of one of the last papers in this series was the two-dimensional registration error, which consists of the longitudinal and lateral registration errors (Brandenburg, 2023). A block diagram had been developed in which the mass flow is closely linked to the generation of the longitudinal registration error, while the lateral one was independent of the mass flow. This simplification does not correspond to physical reality, because changing web tensile forces influence the behavior of the side edges. In the contribution presented here, this dependency is taken into account in an extended model.

1.1 State of the art

In Brandenburg and Klemm (2016), Shelton's beam model (Shelton, 1968) was extended to variable web forces. Variable web forces are caused, apart from technological influences, by changes in the circumferential speeds of rollers that are provided for the transport and processing of the moving web. The equation of the beam bending and the so-called transport equations were linearized. Then additional dynamic terms were found that show the influence of a variable web tensile force during translational or rotational movement of a control roller as well as when a web offset or an angle change was impressed at the entrance to a system.

The numerical example from Brandenburg and Klemm (2016), Figure 6.1.2, led to plausible values of the lateral web deviations. However, it was not possible to verify these results by measurements because no printing press was available. Nevertheless, due to the mentioned plausibility, it makes sense to create a system plan supplemented by the retroactive effect, with the help of which numerous realistic simulations are possible. As in Brandenburg and Klemm (2023), a Bernoulli web is used.

2. Block diagram of the Bernoulli web

2.1 System of notation

In the following, the most important equations of Brandenburg and Klemm (2016; 2019) (in this case for the shear coefficient $a = 1$, valid for the Bernoulli web) are shown.

The system equations that describe the lateral dynamics of the web are the bending equation of the Bernoulli beam (or in the case of Brandenburg and Klemm (2019), the Timoshenko beam) and the two so-called transport equations (velocity equation and acceleration equation)

of the web. At constant transport velocity and constant stress, the bending equation of the Bernoulli beam according to Brandenburg and Klemm (2016), Equation (3.3.1) is

$$\frac{\partial^4 y(x,t)}{\partial x^4} - K_\mathrm{B}^2 \frac{\partial^2 y(x,t)}{\partial x^2} = 0 \qquad [1]$$

with the square of the curvature factor for the Bernoulli web (index 'B')

$$K_\mathrm{B}^2 = \frac{T}{EI} \qquad [2]$$

with

- T: tensile force in newtons [N], affecting beam deformation
- E: modulus of elasticity in pascals [Pa], indicating material stiffness
- I: area moment of inertia about the z-axis in [m^4], reflecting bending resistance.

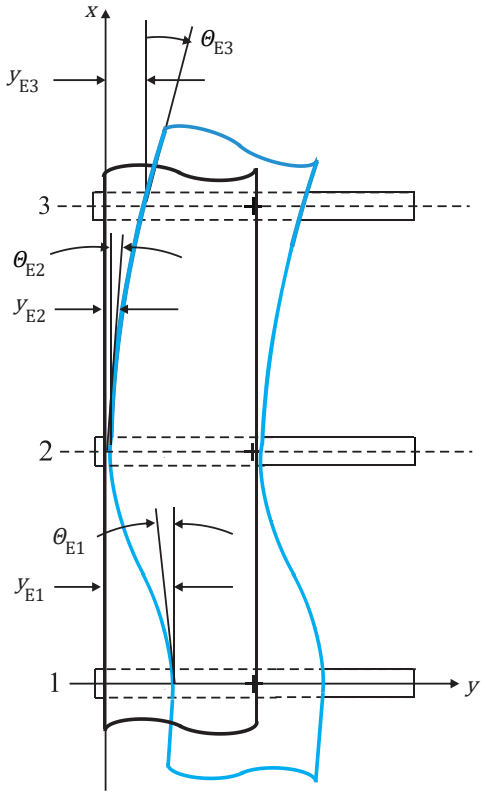

Figure 1: Mathematical notation system for a three-roller system with input offset and change of input angle at roller 1; quantities are given in the List of symbols

In order to introduce variable web velocities and variable tensile forces, Equation [1] must be linearized for small deviations (marked by tilde) from the steady state (marked by horizontal dash), since $K_\mathrm{B} = K_\mathrm{B}(t)$ is a time function now. Linearization was performed in Brandenburg and Klemm (2016).

The linearized form of the Bernoulli web is given by Brandenburg and Klemm (2016), Equation (6.1.4):

$$\frac{\partial^4 \tilde{y}(x,t)}{\partial x^4} - \bar{K}_\mathrm{B}^2 \frac{\partial^2 \tilde{y}(x,t)}{\partial x^2} = \kappa_\mathrm{m} \tilde{T}(t) \qquad [3]$$

with the mean curvature factor

$$\kappa_\mathrm{m} = \frac{1}{EI} \left(\frac{\partial^2 \bar{y}_E(x)}{\partial x^2} \right)_\mathrm{mean} \qquad [4]$$

and the curvature factor

$$\bar{K}_\mathrm{B}^2 = \frac{\bar{T}}{EI} \qquad [5]$$

at the steady-state operating point, as described by Brandenburg and Klemm (2016), Equations (6.1.9) and (2.1.8). Equation [3] is a linear, inhomogeneous differential equation with constant coefficients. This was solved in Brandenburg and Klemm (2016), by the method of variation of the constant (Lense, 1948).

2.2 Transfer functions of the Bernoulli web with variable tensile force and change of position of the control roller

A distinction must be made between two movements of the control roller, namely a pure translation and a pure rotation, because different boundary conditions apply to each of these movements as shown in Brandenburg and Klemm (2016), in Figure 3.3.1, a and b. Accordingly, even in the case of constant web force, there are two separate solutions of the homogeneous, linearized partial differential equation. In the case of variable tensile force, different dynamic terms consequently occur in the case of variable tractive force.

According to Brandenburg and Klemm (2016), Equation (6.3.11) presents the following Laplace-domain transfer function:

$$\tilde{y}_{\mathrm{E3,trans}}(s) = \frac{\frac{\tau_{23}^2}{\bar{f}_{\mathrm{B},23}} s^2 + \bar{K}_\mathrm{B} \tau_{23} s}{\frac{\tau_{23}^2}{\bar{f}_{\mathrm{B},23}} s^2 + \bar{K}_{\mathrm{B},23} \tau_{23} s + 1} \tilde{z}_2(s) + \frac{\frac{L_{23}^2}{\bar{f}_{\mathrm{B},23}} \frac{\mathcal{C}_{5,\mathrm{trans}}^{(23)} \kappa_{\mathrm{m},23}}{\bar{K}_{\mathrm{B},23}^2}}{\frac{\tau_{23}^2}{\bar{f}_{\mathrm{B},23}} s^2 + \bar{K}_{\mathrm{B},23} \tau_{23} s + 1} \tilde{T}_{23}(s) \qquad [6]$$

Equation [6] corresponds to web section 2–3 and assumes pure linear translation of the control roller. In this context, the index 'L' from Brandenburg and Klemm (2016) has been substituted with the web section identifier 23, as depicted in Figure 1. Additionally, Equation (6.3.4) from Brandenburg and Klemm (2016) applies

$$C_{5,\mathrm{trans}}^{(23)} = \left[f_{1T}\bar{K}_{\mathrm{B}}^2 \sinh\bar{u} + f_{2T}\bar{K}_{\mathrm{B}}^2 \cosh\bar{u} + (\cosh\bar{u} - 1) \right]_{23} \quad [7]$$

$\bar{K}_{\mathrm{B},23}^2 = \bar{T}_{23}/(EI)$ according to Equation [6] and Brandenburg and Klemm (2016), Equation (6.1.9), and $\bar{u} = \bar{u}_{23} = \bar{K}_{\mathrm{B},23} L_{23}$ after Brandenburg and Klemm (2019), Equation (3.26).

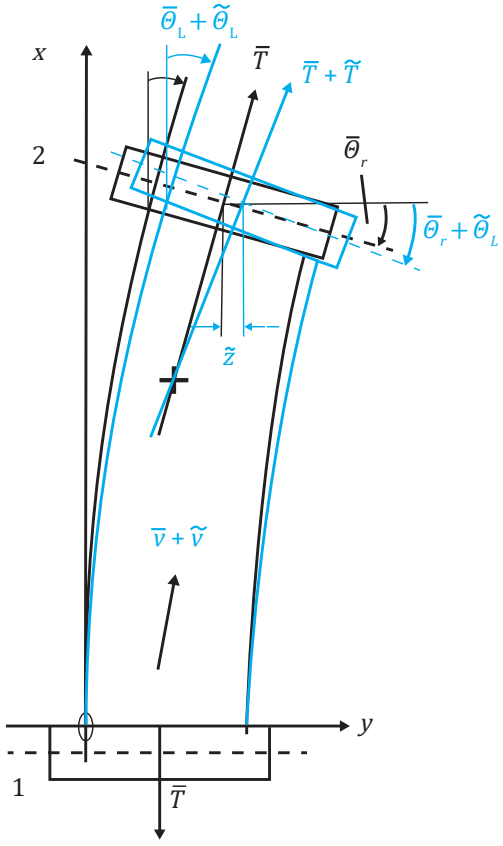

Figure 2: Steady state (black) and small deviations (blue) of the web (from Brandenburg (2016), Figure 6.1.1). Quantities are given in the list of symbols

Since the solution to the homogeneous differential equation (the first term on the right side of Equations [6] and [8]) aligns with the block plan, the second term on the right must also conform to it. This is because the linearized inhomogeneous bending equation from Brandenburg and Klemm (2016), Equation (6.1.10), is structurally composed of the same elements as the homogeneous bending equation in Equation (6.1.2).

The corresponding relations for pure rotation, as described in Brandenburg and Klemm (2016), Equation (6.3.14), are

$$\tilde{y}_{\mathrm{E3,rot}}(s) = \frac{\bar{K}_{\mathrm{B},23}}{\frac{\tau_{23}^2}{\bar{f}_{\mathrm{B},23}} s^2 + \bar{K}_{\mathrm{B},23}\tau_{23} s + 1} L_{23}\tilde{\Theta}_{\mathrm{r2}}(s) + \frac{\frac{L_{23}^2}{\bar{f}_{\mathrm{B},23}} \frac{C_{5,\mathrm{rot}}^{(23)} \kappa_{\mathrm{m},23}}{\bar{K}_{\mathrm{B},23}^2}}{\frac{\tau_{23}^2}{\bar{f}_{\mathrm{B},23}} s^2 + \bar{K}_{\mathrm{B},23}\tau_{23} s + 1} \tilde{T}_{23}(s) \quad [8]$$

with

$$C_{5,\mathrm{rot}}^{(23)} = \left[g_{1T}\bar{K}_{\mathrm{B}}^2 \sinh\bar{u} + g_{2T}, \bar{K}_{\mathrm{B}}^2 \cosh\bar{u} + (\cosh\bar{u} - 1) \right]_{23} \quad [9]$$

Both equations, [6] and [8], consist of the solution of the homogeneous linearized differential equation and of the new term of the change in tensile force.

Now it is necessary to determine at which point in the block plan the variable tensile force $\tilde{\Theta}_{\mathrm{r2}} = 0$ acts. In the first step, the double block plan of Figure 3 is drawn below. The upper part of the plan refers to the pure translation of the control roller, i.e. $\tilde{\Theta}_{\mathrm{r2}} = 0$, the lower part for the pure rotation of the control roller, i.e. $\tilde{z}_2 = 0$.

In the case of pure translation the simpler expression E_{z2} is introduced:

$$\tilde{y}_{\mathrm{E3}}(s) = E_{\mathrm{z2}} A_{23}(s) \tilde{T}_{23}(s) = \frac{1}{\frac{\tau_{23}^2}{\bar{f}_{\mathrm{B},23}} s^2 + \bar{K}_{\mathrm{B},23}\tau_{23} s + 1} E_{\mathrm{z2}} \tilde{T}_{23}(s) \quad [10]$$

with the retro-active factor (c.f. Brandenburg and Klemm (2016), Equation (6.3.12))

$$E_{\mathrm{z2}} = \frac{L_{23}^2}{\bar{f}_{\mathrm{B},23}} \frac{C_{5,\mathrm{rot}}^{(23)} \kappa_{\mathrm{m},23}}{\bar{K}_{\mathrm{B},23}^2} \quad [11]$$

In the case of pure rotation the simpler expression $E_{\theta 2}$ is introduced:

$$\tilde{y}_{\mathrm{E3}}(s) = E_{\theta 2} A_{23}(s) \tilde{T}_{23}(s) = \frac{1}{\frac{\tau_{23}^2}{\bar{f}_{\mathrm{B},23}} s^2 + \bar{K}_{\mathrm{CB},23}\tau_{23} s + 1} E_{\theta 2} \tilde{T}_{23}(s) \quad [12]$$

with the retro-active factor

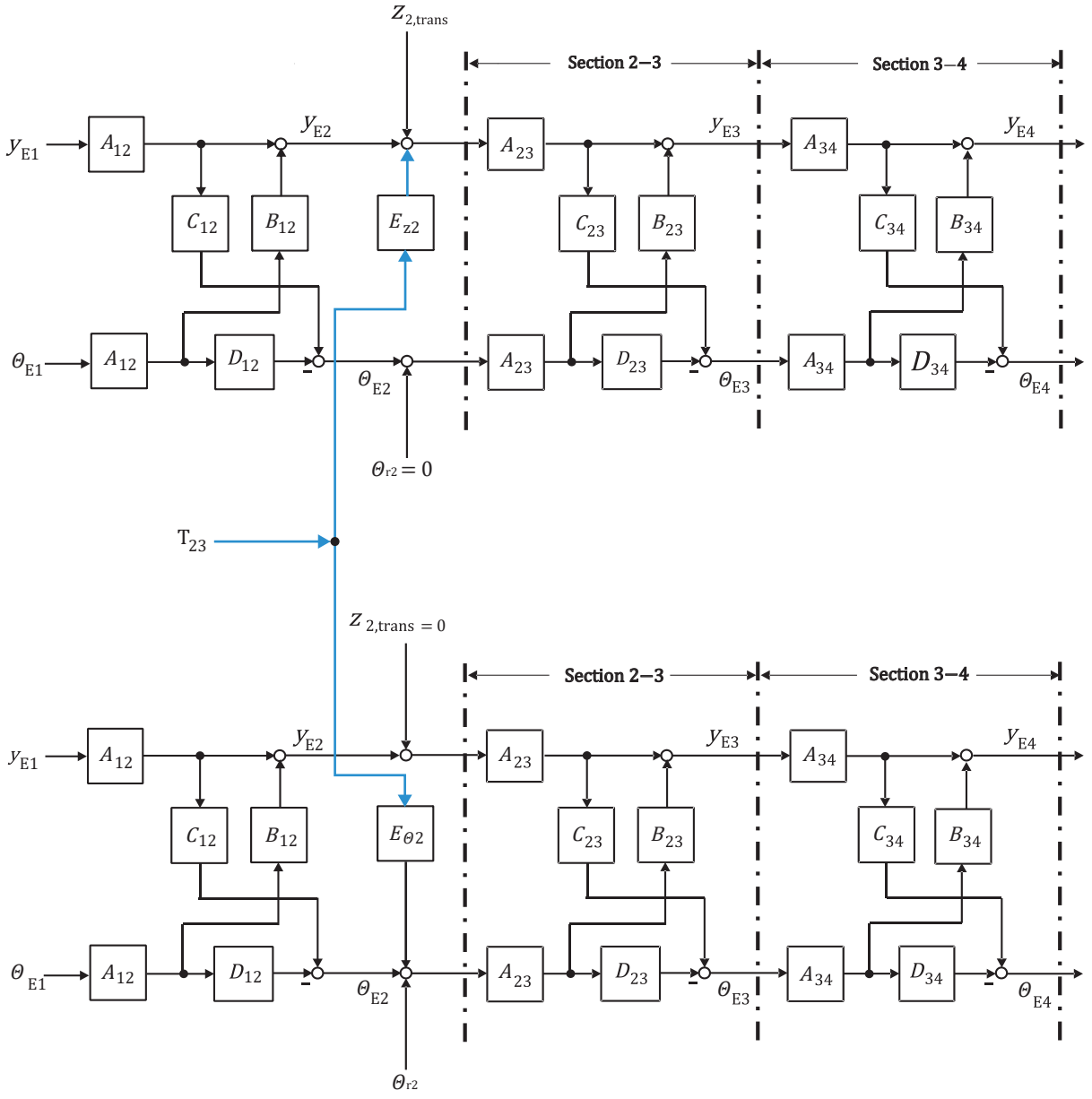

Figure 3. Changes in tensile force (blue) according to the block plan in Brandenburg and Klemm (2019), Figure 5.12; the upper partial block plan is used for pure translation, the lower one for the pure rotation of the control roller; all variables are small deviations from the steady state; quantities are presented in the list of symbols

$$E_{\Theta 2} = \frac{L_{23}^2}{f_{\mathrm{B},23}} \frac{C_{5,\mathrm{rot}}^{(23)} \kappa_{\mathrm{m},23}}{\bar{K}_{\mathrm{B},23}^2} \qquad [13]$$

These terms are shown in Figure 3.

2.3 Transfer functions for input offset and angle change

An input offset and/or a change in input angle were not addressed in Brandenburg and Klemm (2016).

2.3.1 Input offset

If an input offset $\tilde{y}_{E1}$ occurs at roller 1 (see Brandenburg and Klemm (2019), Figure 4.1), and the control roller is in the rest position ($\tilde{z}_2 = \tilde{\Theta}_{r2} = 0$) the input offset is propagated to the entry of roller 2 and triggers both an input offset $\tilde{y}_{E2}$ and a change in the input angle $\tilde{\Theta}_{E2}$.

The upper partial block plan of Figure 3 shows the following: A pure translation $\tilde{z}_{2,\mathrm{trans}}$ dynamically results in

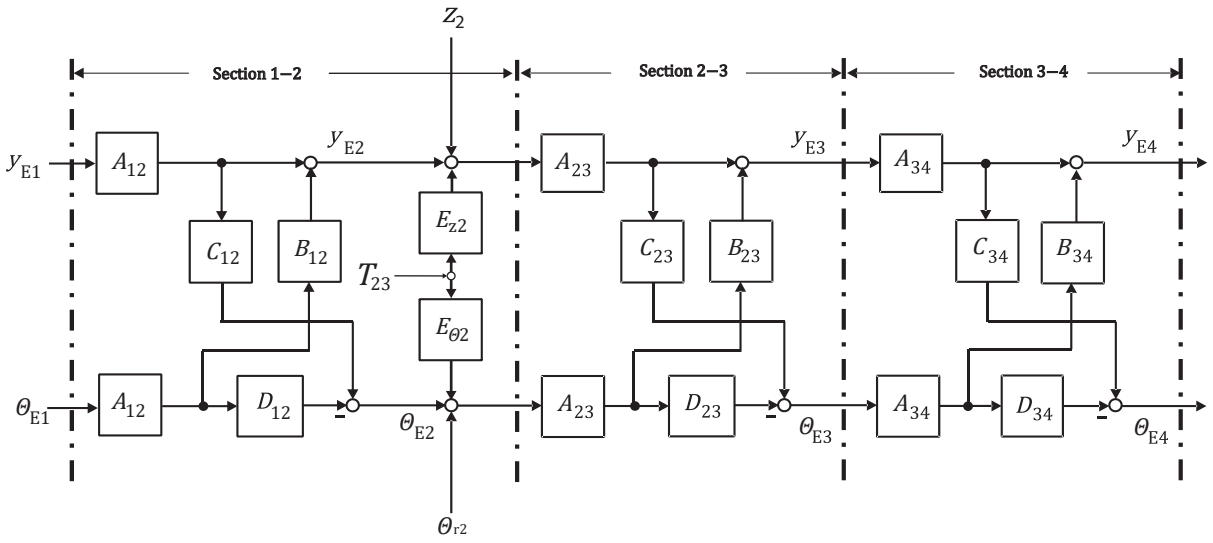

Figure 4. Web tensile force at the summation points of z2 = $z_{(2,\mathrm{trans})}$ and $\Theta_{r2} = \Theta_{(r2,\mathrm{rot})}$. Quantities are presented in the list of symbols

the same dynamic reaction in section 2–3 as an input offset in section 1–2. Therefore, the same equations apply universally, but with appropriately modified transfer blocks. Analogous to Brandenburg and Klemm (2016), Equation (6.3.11), it is written:

$$\tilde{y}_{\mathrm{E2,Evers}}(s) = \frac{\frac{\tau_{12}^2}{f_\mathrm{B}(\bar{u})}s^2 + \bar{K}_\mathrm{B}\tau_{12}s}{\frac{\tau_{12}^2}{f_\mathrm{B}(\bar{u})}s^2 + \bar{K}_\mathrm{B}\tau_{12}s + 1}\tilde{y}_{\mathrm{E1,Evers}}(s) + \frac{\frac{L_{12}^2}{f_\mathrm{B}(\bar{u})}\frac{\underline{C}_{5,\mathrm{Evers}}^{(12)}\kappa_\mathrm{m}}{\bar{K}_\mathrm{B}^2}}{\frac{\tau_{12}^2}{f_\mathrm{B}(\bar{u})}s^2 + \bar{K}_\mathrm{CB}\tau_{12}s + 1}\tilde{T}_{12}(s) \quad [14]$$

$$\underline{C}_{5,\mathrm{Evers}}^{(12)} = \left[f_{1T}\bar{K}_\mathrm{B}^2\sinh\bar{u} + f_{2T}\bar{K}_\mathrm{B}^2\cosh\bar{u} + (\cosh\bar{u} - 1)\right]_{12} \quad [15]$$

and $\bar{K}_\mathrm{B}^2$ according to Equation [3]. The first term on the right indicates that for $t \to \infty$ the input offset has arrived at the input of roller 2. The second term describes the influence of the variable tensile force on the input of roller 2 and comes from Brandenburg and Klemm (2016), Equation (6.3.11), and Equation [14] is identical to the second term of Brandenburg and Klemm (2019), Equation (4.83) when formulated for the Bernoulli web.

2.3.2 Change of the input angle

The following can be seen in the lower partial block plan of Figure 3: A pure change in angle $\tilde{\Theta}_{r2}$ results in the same dynamic reaction in section 2–3 as a change in the input angle $\tilde{\Theta}_{E1}$ for section 1–2. Therefore, the same equations apply, but with modified transfer blocks. Analogous to Equation (6.3.14) in Brandenburg and Klemm (2016) it is written:

$$\tilde{y}_{\mathrm{E2,Ewinkel}}(s) = \frac{\bar{K}_\mathrm{B}(\bar{u})}{\frac{\tau_{12}^2}{f_\mathrm{B}(\bar{u})}s^2 + \bar{K}_\mathrm{B}(\bar{u})\tau_{12}s + 1} \times L_{12}\tilde{y}_{\mathrm{E1,Ewinkel}}(s) + \frac{\frac{L_{12}^2}{f_\mathrm{B}(\bar{u})}\frac{\underline{C}_{5,\mathrm{Ewinkel}}^{(12)}\kappa_\mathrm{m}}{\bar{K}_\mathrm{B}^2}}{\frac{\tau_{12}^2}{f_\mathrm{B}(\bar{u})}s^2 + \bar{K}_\mathrm{B}(\bar{u})\tau_{12}s + 1}\tilde{T}_{12}(s) \quad [16]$$

with

$$\underline{C}_{5,\mathrm{Ewinkel}}^{(12)} = \left[g_{1T}\bar{K}_\mathrm{B}^2\sinh\bar{u} + g_{2T}\bar{K}_\mathrm{B}^2\cosh\bar{u} + (\cosh\bar{u} - 1)\right]_{12} \quad [17]$$

Then the two partial block plans from Figure 3 can be pushed one on top of the other to create Figure 4, in which the change in tensile force $\tilde{T}_{23}(s)$ acts in the middle between the blocks E_{z2} and $E_{\theta 2}$. In the model according to Brandenburg and Klemm (2019), Figure 5.5, it is assumed that when the input offset and/or input angle change is assumed, the control roller 2 (see Figure 5) is in the rest position.

The question of what kind of transient would occur if the control roller is at rest but at an angle, i.e. has a stationary position $\bar{\Theta}_{r2} \neq 0$, is not relevant. This is because

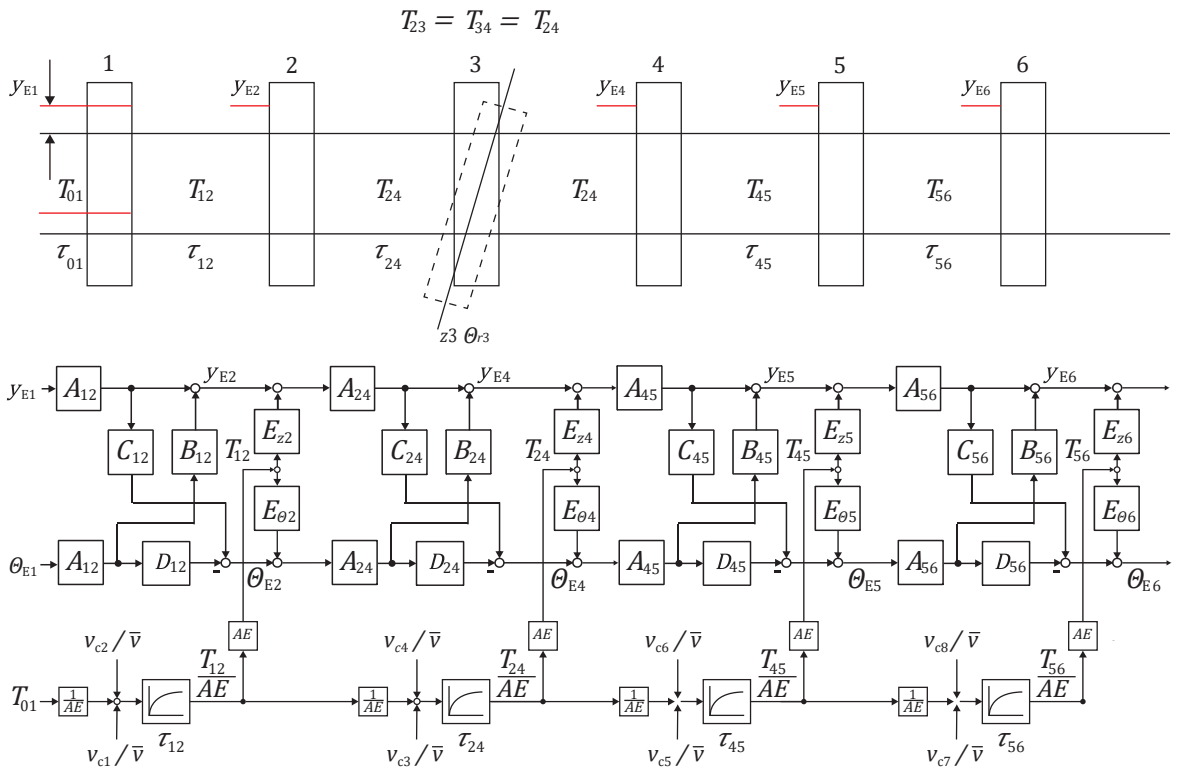

Figure 5: Complete system with control roller and mass flow chain; all variables are small deviations from the steady state; quantities are presented in the list of symbols

it is an initial state that influences the stationary movement of the web, but which no longer plays a role after the introduction of small deviations.

2.4 Relationship of tensile force with the continuity equation

2.4.1 Transfer functions of the lateral behavior under the influence of control rollers

The following consideration is important: The three-roller system in Figure 1 assumes that there is a change in tensile force $\tilde{T}$ on roller 2, which is accompanied by a change in the speed of the web. The main reason for this is not important for this particular discussion.

2.4.2 Mass flow in the six-roller system and reaction to lateral movement

So far, the causes of a change in web force have not been discussed, but rather how this affects lateral web deviation has been investigated.

Changes in web tension and web force are – apart from changes in humidity and temperature – caused by the mass flow, for example by changing the peripheral speeds of the drive rollers, as is well known. The mathematical description is based on the continuity equation. This concept was already derived in Brandenburg (1976). In contrast to German literature, it has hardly played a role in American engineering literature. Anyhow, in recent years, interest in applying these principles to high-speed web handling has grown.

For Bernoulli webs, i.e. webs that are not too wide ($L/b > 10$, where L is the length and b the width of the web, i.e. by definition its shear factor is $a = 1$) can be shown that:

- The equations of the lateral behavior of the web and the mass flow are only slightly coupled to one another,
- There is hardly any difference between the continuity equation in the x-direction and the slightly different lateral transport direction.

A six-roller system according to Figure 5 with control roller 3 is assumed. In this case, the mass flow chain drawn in Figure 6 follows from Equation [18].

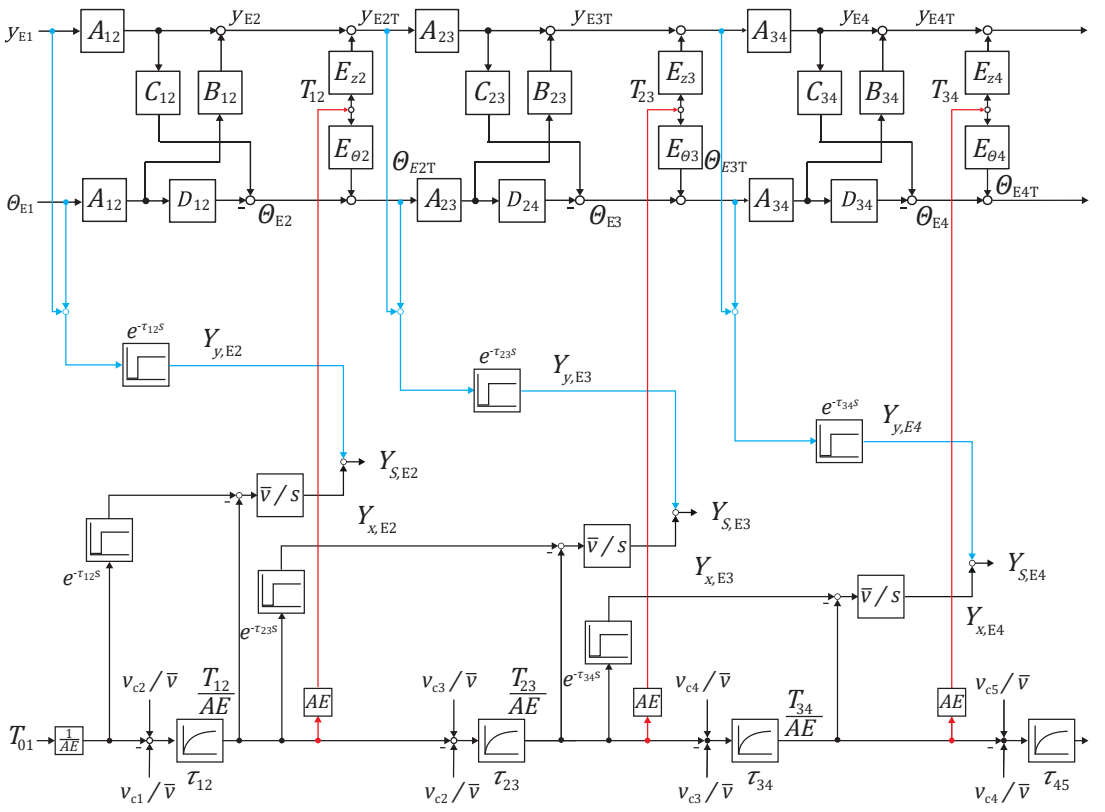

Figure 6: Block plan of the overall system without control roller (blue signal lines: lateral register errors, black signal lines: longitudinal register errors, red signal lines: retroactive effect of the web tensile forces); ; quantities are presented in the list of symbols

$$\tilde{\varepsilon}_{i,i+1}(s) = \frac{1}{1+\tau_{i,i+1}s} \times \left[\tilde{\varepsilon}_{i,i-1}(s) + \frac{\tilde{v}_{c,i+1}(s) - \tilde{v}_{c,i-1}(s)}{\bar{v}}\right] \quad [18]$$

The tensile force $\tilde{T}_{01}$ is impressed on the roller 1. The control roller 3 is positioned between the axially driven rollers 2 and 4. The rollers 5 and 6 are also axially driven rollers. Each web section is represented by a PT1 element (i.e. a 1st order lag) with a time constant according to Equation [18]. These PT1 elements act on the lateral deflection and the angular deviation of the actual web.

The strain was written in the form

$$\tilde{\varepsilon}_{i,i+1} = \frac{\tilde{T}_{i,i+1}}{AE} \quad [19]$$

Since the movement of the control roller has no influence on the web tension, the web tension in sections 2–3 and 3–4 is the same. The question now is whether every lateral deviation $\tilde{y}_{Ei}$ and every change in angle $\tilde{\Theta}_{Ei}$ can be assigned a reaction from the material flow chain. The answer is that this is mandatory. For example, it may be that $\tilde{T}_{01} = 0$ and only the speed $\tilde{v}_{c5} \neq 0$ changes. Then there is always a reaction on $\tilde{y}_{E5}$ and $\tilde{\Theta}_{E5}$ (see Figure 5).

The next step is to add the register errors to the block plan from Figure 5.

2.5 Registration errors taking into account the retro-active effects of variable web tensile forces

In the publication Brandenburg and Klemm (2023), Figure 4, there is already a system plan with lateral and longitudinal registration errors, which, however, does not take into account the effects of changes in tensile force on the lateral behavior of the web. Figure 5 presented here has been supplemented with the additional blocks of register errors, without the control roller for reasons of clarity. This creates the 'multi-layer plan' presented in Figure 6.

In the 'cycle' of the mass flow chain, the lateral web deviations and thus the lateral register errors are influenced via the signal paths marked in red.The longitudinal register errors due to the force changes in the mass flow chain are well known. When adding the longitudinal and the lateral register error, it must be noted that the two

errors are perpendicular to each other (Brandenburg and Klemm, 2023).

If the mass flow chain is only excited by $\widetilde{T}_{01}$, the three longitudinal register errors $\widetilde{Y}_{x,\mathrm{E2}}$, $\widetilde{Y}_{x,\mathrm{E3}}$ and $\widetilde{Y}_{x,\mathrm{E4}}$ appear. The retro-active signal paths (red in Figure 5) produce the lateral register errors $\widetilde{Y}_{y,\mathrm{E3}}$ and $\widetilde{Y}_{y,\mathrm{E4}}$, without any change in $\widetilde{y}_{\mathrm{E1}}$ or $\widetilde{\Theta}_{\mathrm{E1}}$. The lateral register error $\widetilde{Y}_{y,\mathrm{E2}}$ also occurs, only if $\widetilde{y}_{\mathrm{E1}} \neq 0$ and/or $\widetilde{\Theta}_{\mathrm{E1}} \neq 0$ is valid.

The following engineering and scientific results are completely new.

The multi-layer model of Figure 6 did not yet exist in this form. It consists of three layers, which can be characterized as follows:

1) In the upper layer, it shows the linkage of the lateral deflections and input angle changes according to the lateral block plan.

2) In the lower layer it shows the link of the longitudinal strain changes $\varepsilon_{i,i+1} = \widetilde{T}_{i,i+1}/(AE)$ with the peripheral velocities of the longitudinal time lags. And it is an image of the mass flow.

3) The middle layer consists of the lateral register errors $\widetilde{Y}_{y,\mathrm{E}}$ and the longitudinal register errors $\widetilde{Y}_{x,\mathrm{E}}$.

Their sum makes up the total register errors $\vec{\widetilde{Y}}_{S,\mathrm{E}}$. When adding, it should be noted that they are spatially perpendicular to each other. Therefore, they can also be written vectorially, as Equation [20] shows (Brandenburg and Klemm, 2023):

$$\vec{\widetilde{Y}}_{S,\mathrm{E}i} = \vec{\widetilde{Y}}_{x,\mathrm{E}i} + \vec{\widetilde{Y}}_{y,\mathrm{E}i} = \widetilde{Y}_{x,\mathrm{E}i}\vec{e}_x + \vec{\widetilde{Y}}_{y,\mathrm{E}i}\vec{e}_y \qquad [20]$$

This sum vector changes its magnitude and angle during a transient while the web is moving.

The multi-layer model shown in Figure 6 can be regarded as a new module of the automation technology.

2.6 Potential of the multi-level model

The multi-level model shown in Figure 6 offers a comprehensive application potential for simulations and subsequent measurements:

- Change of one or all three input variables: web offset, input angle and tensile force,
- Change of peripheral velocities of the mass flow chain and investigation of their effect on the other variables of the overall system,
- Extension of Figure 6 to include the partial cutting register errors (Brandenburg, 2011),
- Insertion of the mathematical models for doubling in and between printing units (Brandenburg 2000),
- Extension of Figure 6 by the electronic line shaft of the controlled drive motors,
- Insertion of side edge controls of the web,
- Insertion of the controls for longitudinal and/or lateral register errors,
- Non-interacting control of web forces and cut-off register errors in rotary printing presses with electronic line shafts (see Brandenburg, Geißenberger and Klemm, 2004),
- Investigation of controls of tensile forces.

3. Conclusion

The state-of-the-art printing press is a system consisting of printing units that print information on the moving web and of electric drive motors in the form of an electronic line shaft. Together with guide rollers these units provide high-precision longitudinal and lateral web guidance. Because of multiple disturbances, longitudinal and lateral register errors occur. In order to keep these register errors to a minimum, the disturbances must be minimized on the one hand by technological measures and on the other hand by means of closed-loop controls.The multi-layer model in Figure 6 shows the overall system of lateral and longitudinal register errors in a clear manner as well as the retro-active effect of the mass flow chain on the lateral register errors. The multi-layer model enables extensive simulations of the relevant system variables with the aim of reducing time-consuming measurements on real printing machines. In the case of printing companies with large pressroom equipment, e.g. with machines for commercial printing, machines for newspaper printing, and rotogravure presses for high-quality art printing, the multi-layer model, together with other production elements, could be fed into an AI that carries out higher-level operational coordination tasks (see also Chen, 2023).

Acknowledgement

I would like to express my sincere thanks to Dr. Andreas Klemm for carrying out the formatting guidelines and for fruitful discussions over many years for numerous publications.

List of symbols

a	Shear coefficient
b	Width of the web
$\underline{C}^{(23)}_{5,\mathrm{trans}}$, $\underline{C}^{(23)}_{5,\mathrm{rot}}$	Constants for pure translation and pure rotation, respectively, in web section 2–3 according to Equations [7] and [9]
E	Modulus of elasticity
E_{z2}	Retro-active factor of tensile force on the lateral web deflection, Equation [11]
$E_{\Theta 2}$	Retro-active factor of tensile force on the lateral web angle change, Equation [13]
$\bar{f}_{\mathrm{B},i,i+1}$	Steady state constant of the Bernoulli web in section $i, i+1$, Equations [6] and [8]
f_{1y}, f_{2y}	Constants according to Brandenburg and Klemm (2016), Equations (3.3.1.6), (3.3.1.7) and (6.2.6)
f_{1T}, f_{2T}	Constants according to Brandenburg and Klemm (2016), Equations (6.2.9) and (6.2.10)
g_{1T}, g_{2T}	Constants according to Brandenburg and Klemm (2016), Equations (6.2.18) and (6.2.19)
$g_{1\Theta}, g_{2\Theta}$	Constants according to Brandenburg and Klemm (2016), Equations (6.2.18) and (6.2.19)
h	Thickness of the web
I	Moment of inertia of area referred to the z-axis in [m^4]
K_{B}	Curvature factor $K = \sqrt{T/EI}$ in [m^{-1}] for the Bernoulli web
$K_{\mathrm{B},i,i+1}$	Curvature factor (of the Bernoulli web) in section $i, i+1$
$\bar{K}_{\mathrm{B}}$	Steady state curvature factor according to Brandenburg and Klemm (2016), Equation (2.1.8) and Equation [5]
$L_{i,i+1}$	Length of the free web between rollers $i, i+1$
s	Laplace transform operator
t	Time
T	Tensile force [N] according to Brandenburg and Klemm (2016), Figure 2.1.2
$\tau_{i,i+1}$	Time constant of the web in section $i, i+1$
$\widetilde{T}_{23}(s)$	Small variation of tensile force in section 2-3
$\bar{u}_{i,i+1}$	From curvature factor and length: $\bar{u}_{L,i,i+1} = \bar{K}_{\mathrm{B},i,i+1} L_{i,i+1}$ in web section $i, i+1$, according to Brandenburg and Klemm (2019), Equation (3.26) in steady state of motion
V	Velocity in direction of web motion (see Brandenburg and Klemm (2016), Figure 2.1.1)

$V_{\mathrm{C}} = v_{\mathrm{C}} \approx V$	Peripheral velocity of the control roller 2 (velocity of the web elements in the adhesion zone of the control roller ≈ web velocity, see Figure 2.1.1, Shelton 1968)
(x, y)	Coordinate system (see Figure 1)
y_{E}	Lateral web deflection (see Figure 1)
$y_{\mathrm{E}i,\mathrm{trans}}$	Lateral web deflection at entry i with translatory movement
$y_{\mathrm{E}i,\mathrm{rot}}$	Lateral web deflection at entry i with rotational movement
$y_{\mathrm{E2,Evers}}$	Lateral web deflection at entry i with input offset
$y_{\mathrm{E2,Ewinkel}}$	Lateral web deflection at entry i with change of the input angle
$\widetilde{Y}_{x,\mathrm{E}i}$	Longitudinal registration error at entry of roller i (see Figure 6)
$\widetilde{Y}_{y,\mathrm{E}i}$	Lateral registration error at entry of roller i (see Figure 6)
$\widetilde{Y}_{S,\mathrm{E}i}$	Lateral registration error (cf. Figure 6 and Equation [20])
z	Lateral position of roller 2 (see Figure 2)
Θ_{E}	Entry angle (see Figure)
Θ_L	Angle of web edge relative to x-axis at the entrance line of roller 2 (see Figure 2)
Θ_{r}	Rotation angle of the control roller (see Figure 4)

References

Brandenburg, G. and Tröndle, H.-P., 1976a. Dynamik des Längsregisters bei Rollenrotationsdruckmaschinen: Teil 1. *Siemens Forschungs- und Entwicklungsberichte*, 5(1), pp. 17–20.

Brandenburg, G. and Tröndle, H.-P., 1976b. Dynamik des Längsregisters bei Rollenrotationsdruckmaschinen: Teil 2. *Siemens Forschungs- und Entwicklungsberichte*, 5(2), pp. 65–71.

Brandenburg, G., 2000. Dynamisches Verhalten von Dublier- und Registerfehlern bei Rollenoffset Druckmaschinen. In: *Tagungsband SPS/IPC/DRIVES 2000*. Nürnberg, Germany, 28–30 November 2000. Heidelberg: Hüthig-Verlag, pp. 698–715.

Brandenburg, G., Geißenberger, S. and Klemm, A., 2004. Noninteracting control of web forces and cut-off register errors in rotary printing presses with electronic line shafts. In: *11th Int. Power Electronics and Motion Control Conference EPE-PEMC*. Riga, Latvia, Vol. 6, pp. 6-35 to 6-42.

Brandenburg, G., 2011. Advanced process models and control strategies for rotary printing presses. In: *Proceedings of the 11th International Conference on Web Handling*. Stillwater, OK, USA, 12–15 June 2011. Stillwater: Oklahoma State University.

Brandenburg, G. and Klemm, A., 2016. Lateralverhalten kontinuierlicher elastischer Bahnen, Kurzfassung des Balkenmodells von Shelton und Erweiterung auf variable Bahnzugkraft. In: U. Fügmann, ed. 2016. *Proceedings zum 13. Bahnlaufseminar,* Chemnitz, Germany, 19–20 September 2016. Berlin: VWF Verlag für Wissenschaft und Forschung 2017. pp. 35–104.

Brandenburg, G. and Klemm, A., 2019. Lateralverhalten elastischer Bahnen bei Berücksichtigung des Schubeinflusses. In: U. Fügman, ed. *Modellbildung und Simulation: Proceedings zum 14. Bahnlaufseminar 2018*. Chemnitz, Germany, 18–19 September 2018. Berlin: VWF Verlag für Wissenschaft und Forschung, pp. 53–150.

Brandenburg, G., 2023. Two-dimensional register error. *Journal of Print and Media Technology Research*, 12(3), 127–133. https://doi.org/10.14622/JPMTR-2303.

Chen, Z., 2023. Control of high precision roll-to-roll printing systems. PhD., University of Michigan, Horace H. Rackham School of Graduate Studies. https://doi.org/10.7302/8576.

Lense, J., 1948. Vorlesungen über höhere Mathematik. München, Leibnitz Verlag.

Shelton, J. J., 1968. Lateral dynamics of a moving web. PhD., Oklahoma State University, Stillwater, OK, USA.

JPMTR-2412
DOI 10.14622/JPMTR-2412
UDC 667.2:535.6:676.2+678.7+66.095

Review paper | 194
Received: 2024-10-10
Accepted: 2024-12-27

Natural plant dye inks set new challenges: analysing the interaction of anthocyanin-rich dye with modern calcium carbonate containing substrates

Katarina Dimić-Mišić [1,2], *Monireh Imani* [1,3] *and Patrick A.C. Gane* [1,4]

[1]School of Chemical Enhgineering,
Department of Bioproducts and Biosystems,
Aalto University, 00076 Aalto, Finland
[2]Institute of General and Physical Chemistry,
Studentski trg 12/V, 11158 Belgrade, Serbia
[3]Mirka Ltd., Pensalavägen 210, 66850 Jeppo, Finland
[4]Faculty of Technology and Metallurgy,
University of Belgrade, Karnegijeva 4, 11200 Belgrade, Serbia

katarina.dimic-misic@aalto.fi
monireh.imani@mirka.com
patrick.gane@aalto.fi

Abstract

Plant dyes are increasingly finding applications across a broad spectrum of print technologies, leading to replacement of conventional synthetic dyes and pigmented inks for a range of print media. Despite technical advances, industrial application faces some fundamental challenges of achieving the necessary critical print properties demanded when using such dyes. These include maintaining runnability, colour definition and fastness while retaining functional stability, the latter being particularly challenging since many prints are based on digital patterning adopting inkjet or flexographic methods. This study explores the fundamental interactions between an example pure dye ink, derived from Aronia melanocarpa, a member of the family Rosaceae commonly known as chokeberry, and specific substrate filler and coating components. Key interactive factors include ink formulation, the nature of dye chemistry in relation to substrate structure, its optical properties and constituent components. The acidity of the juice-based ink is mainly dependent on the amount of anthocyanin (ANC), a water-soluble phytochemical plant protective flavonoid, occurring together with other phenolic compounds. Novel experiments are reported in which interactive substrate components are isolated and studied directly in contact with the naturally acidic anthocyanin-rich ink. Coloration of the dye is confirmed to be pH-dependent, and, as a result, major challenges arise when acidic ink contacts alkaline substrate, which covers the majority of paper, board and cellulose-based packaging materials today, due to the dominance of calcium carbonate as the filler and coating pigment of choice. In parallel, dye imbibed into substrate pores surrounded by materials of contrasting refractive index lead to effective colour gamut changes as the ratio of transmitted light through dye and scattered light from surrounding materials changes. This effect is exemplified comparing high refractive index titanium dioxide (TiO_2) versus lower refractive index calcium carbonate ($CaCO_3$). Finally, a strategy is proposed aimed at controlling the interaction and enhancing the overall printing performance.

Keywords: Aronia melanocarpa, ANCs, inkjet printing, solar cells, rheology of printing inks, edible printing.

1. Introduction

Printing of biobased inks, derived from fruits and vegetables, have been attractive for numerous applications, including in food production, for smart packaging on flexible paper and board substrates and for highly functional photocatalytic devices (Hakim,, et al., 2024; Tahir and Saad, 2021). Employing the sensitivity of natural dyes to their environment has been the driver in the case development of smart packaging for food, providing the potential of indicating shelf-life of perishable goods, as summarised in the review by Singh, Gaikwad and Lee (2018), covering the study of anthocyanin (ANC) dye. Photoselectivity of natural dyes features in their

role in organic solar cell production. This latter example is currently of major importance, since the growth of modern industry is highly dependent on establishing the use of renewable raw material and energy sources. Existing natural resources for fuel continue to diminish, and the building of a renewable energy based sustainable economy is vital to fulfil the production, transportation, and industrial trade needs of a growing global population (Perišić,, et al., 2022). Solar energy is clearly among the fastest growing proposed methods of capturing renewable energy. The typical lifespan of modern solar panels is 20–30 years. However, as solar deployments increase, a significant wave of decommissioned panels is expected in the coming decades, creating a potential waste management challenge (Huang, et al., 2022). The industry continues to focus on recycling concepts and repurposing of materials from decommissioned panels in an an effort to create circular economy. One contribution to sustainability is the adoption of biobased inks and substrates (Wathon, et al., 2019).

Adhesion in the case of dye inks is additionally related to adsorption onto surfaces, and the capture of dye in this way is very important in defining the position of the dye on and in the substrate and as a separating function for dye from solvent. The required adhesion of inks to paper can be affected by ink formulation, i.e. colorants, solvents, and diluent or carrier vehicle, and its interaction with the substrate pore structure (Ridgway and Gane, 2005). The influence on ink colorant distribution and adhesion mostly depends upon the compatibility between the dye and the carrier vehicle system, concentration and degree of dispersion in the final ink (Jurič, et al., 2013) and in parallel, the adsorption properties onto the substrate material surfaces, and, in the case of porous substrates, including pore wall adsorption (Ridgway and Gane, 2005). Distribution on non-absorbent substrates is controlled by the wetting behaviour of the ink vehicle solvent and finally the film-forming ability of the ink binder resin and its molecular affinity for the substrate, whilst distribution on and within a porous substrate is influenced additionally by the degree of vehicle penetration, transporting colorant into the pore structure – all major features particularly important for sustainable functional printing (Arya, et al., 2024). Solvents can, therefore, affect the distribution of printing ink in two different ways, demanding designed control of both wettability and penetration. Optimal control of ink penetration into the substrate surface without complete loss into the bulk can assist physical and chemical bonding and generate maximum coloration efficiency (Gane and Koivunen, 2010; Koivunen and Gane, 2010). The pore space and chemical properties of particulate grain surfaces are, therefore, important properties of a porous print substrate. Printing technology also places different demands on the interaction of liquid ink and a substrate. One of the most challenging is that of inkjet, a technology that has many advantages when considering functional print applications, due to its flexibility in handling readily modified ink formulations, particularly dye-based inks, and in small quantities for specialisation (Gane, et al., 2021; Dimić-Mišić, et al., 2015). Droplets of ink on arrival at the surface of the substrate are subject to wetting and capillary forces resulting in the solvent vehicle part of the ink together with the ink dye becoming absorbed into the fine pore structure, and thus separated from pigments, or pigment aggregates, and solid phase binders larger the pores (Gane, et al., 2021).

In the field of health foods and nutraceuticals, phenolic acid and polyphenols in general are well known for their anti-oxidant properties (Ebrahimi and Lante, 2021). Many nutraceutical products use printing techniques, including 3D printing, to incorporate active agents. This is common when formulating tablets with alkali calcium carbonate as an excipient. In these cases, the pH sensitivity of dye molecules is also crucial (Cotabarren, Cruces and Palla, 2019). In this field, traditional remedies for hypertension based on these compounds have been gaining recent attention. Surprisingly, the finding that polyphenols lower blood pressure, although seeming to be quite recent, and certainly long after the ailment was defined via blood pressure measurement (1856), ancient peoples native to the Americas (Abnakians and Potawatomians) (Rousseau, 1945; Rousseau, 1947; Smith, 1933) were using it medicinally for the treatment of cold, but probably did not know the link to the cause of whatever symptoms they were displaying (Hellström, et al., 2010). Similarly, in Russia and Lithuania chokeberry fruits have been used as antisclerotic agents as well as a complementary remedy against high blood pressure (Henneberg and Stasrznewicz, 1993; Sokolov, 2000).

In light of the traditional uses of chokeberry, it has been recently confirmed that it is one of the most prolific sources among plant berries, from which typically ~ 100 mg can be recoverable from 100 g of the plant's berry fruit (Tolić, et al., 2015). The rich content in natural compounds like polyphenols, flavonoids, and antioxidants not only enhance the overall health of the plant but also fortify it, with the leaves and stems being of a robust and tough texture, diminishing their appeal to many pests (Sant'Anna, et al., 2013; Zdunić, et al., 2020; Živković, et al., 2020; Zhang, et al., 2023). Unlike softer plants that insects find easier to penetrate and feed on, the resilience of its foliage acts as a formidable physical barrier. We also study two examples of the dye from different geographical regions, and so the geographical distribution differences are partly explained from the history of the plants involved. The berry originally proliferated in the eastern parts of North America, concentrated in Eastern Canada, and arrived in Europe as late as around 1900, passing through Germany to the then

Soviet Union (Russia) around 1946, during which time the plant was established as a cultivar. Aronia plants display ready adaptability to diverse soil conditions and climates, a trait closely tied to their resilience against pests. This adaptability enables them to flourish in different environments, withstanding potential stressors that might compromise the health of other plants. More recently it is being cultivated also in East European and Scandinavian countries, with the genus name Aronia being used instead of the original colloquial name, chokeberry. Aronia is a member of the Rosaceae family, and the cultivars used for fruit production are from the species Aronia melanocarpa, Elliot (black chokeberry, Aronia noir) and Aronia arbutifolia, originally from North America now cultured in the Baltic countries (Mossberg, et al., 2005; McKay, 2001).

Aronia shrubs, capable of reaching heights between 2 to 3 m, produce umbels comprising approximately 30 small white flowers from May to June. These flowers eventually give rise to two types of berries: bright red berries (red chokeberry) or purple-black berries (black chokeberry) that have diameter typically 6 to 13 mm and a weight ranging from 0.5 to 2 g. Harvesting, which is typically mechanised, is between August and September (Živković, et al., 2020).

The main compounds in Aronia berry juice are benzaldehyde cyanohydrin, hydrocyanic acid, and benzaldehyde. Among the benzene derivatives mostly present are to be found benzylalcohol, 2-phenylethanol, phenylacetaldehyde, salicylaldehyde, acetophenone, 2′-hydroxyacetophenone, 4′-methoxyacetophenone, phenol, 2-methoxyphenol and methyl benzoate. ANCs, also present as a group of plant molecules, are the components responsible for the colour of various fruits and flowers, protecting the plants from damage due to UV radiation (Huang and Xu, 2023). Chemical aspects of ANC are defining the colour of juice and colour durability, and these aspects largely define utilisation of Aronia in food applications. The typically purple-black fruit is an abundant source of dye colorant, and so is of major interest in the forming of dye-based printing ink.

A current challenge when using plant-based dyes is to maintain their colour properties, which degrade as a function of enzymatic breakdown. The resulting observed browning of fruit products is naturally detrimental to the appearance since it results in an undesirable colour change. However, colorants rich in phenols when combined with high levels of co-pigment/pigment ratio show a remarkable colour stability. In this context, it was found that chlorogenic acid, at concentrations greater than that of the natural ANCs present, enhanced the colour intensity of Aronia juices, suggesting the participation of natural pigments present in fruits in maintaining a co-pigmentation process (Dangles, Saito and Brouillard, 1993). By contrast, catechins appear to have a negative effect on red colorants, quickly turning yellowish when the pH is increased, whilst the presence of sugars is not influencing the colour. At a given pH, colour stability mainly depends on the structures of ANCs and of colourless phenolic compounds. Colorants rich in acylated ANCs (purple carrot, red radish, and red cabbage) display great stability due to intramolecular co-pigmentation. In aqueous solutions, aglycones of ANCs, organic compounds, such as a phenol or alcohol, combined with the sugar portion of a glycoside which exist as five molecular components, are held in chemical equilibrium. The colour gamut can range from red flavylium cation, through colourless carbinol pseudo base, to purple quinoidal base, blue quinoidal anion, and yellowish chalcone (Dangles, et al., 1993). Anthocyanins derived from the respective aglycones (anthocyanidins), and the general structure (flavylium cation), are shown in Figure 1 a) and c) (Mary, et al., 2020). At acidic pH (pH 2.0), flavylium cation is the dominant form and has a strong absorption at 520 nm, displaying a red colour. Changes can occur as pH rises with the flavylium cation losing proton and

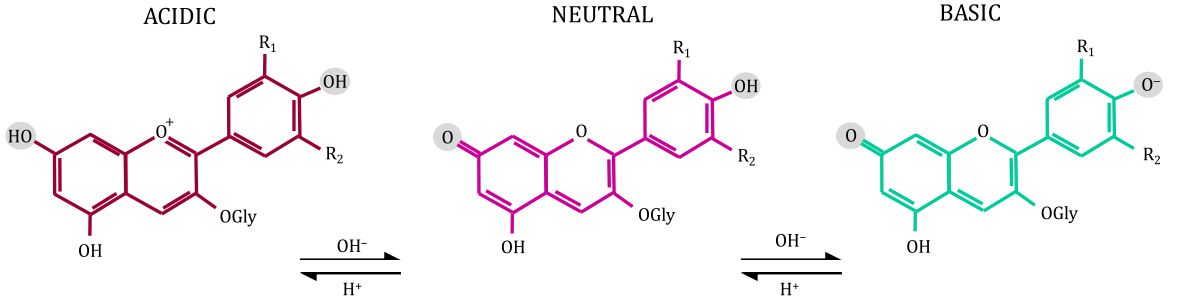

Figure 1: Effects of pH of anthocyanin colour ranges and shift from red to blue at increasing pH; red colour that turns into purple at pH 1–5 (a), purple colour that turns into brown at neutral pH 6–9 (b), and green colour that turns to yellow at basic pH of 10–13 (c) [Figure taken and modified from (Mary, et al., 2020): [14] Open Access Article licensed under a Creative Commons Attribution-Non Commercial 3.0 Unported Licence – one change made applying equivalent chemistry replacing – H^+ with OH^- to indicate the same addition of base.]

gradually converting to quinoidal bases. The visible light spectral absorption becomes much weaker and shifts to 540–560 nm, yielding a red (pH 4.0) or a purple (pH 6.0) colour. At neutral pH, the blue quinoidal anion forms by losing another proton, and as a result reveals a stronger, red-shifted absorption reaching ~600 nm maximum. Ultimately, under basic conditions (pH > 8.0), i.e., passing through pH values typical of alkaline natural calcium carbonate, the flavylium cation will dehydrate to form colourless carbinol pseudo base and then chalcone. The chalcone form is yellow in colour, related to its absorption in the UV and violet-blue regions. The green colour of the anthocyanin solution at even higher pH 10.0 is derived from a resulting mixture of blue quinoidal anion and yellow chalcone (Mary, et al., 2020).

Upon digestion by endogenous enzymes in the human gastrointestinal tract, ANCs are released from the berry structure (Fu, et al., 2023). Anthocyanin in solution is changing both in respect to food health properties and in coloration as pH rises. During the progressive neutralisation of phenolic acids, a salt is formed. Under strongly alkaline conditions organic acids in general attach to sugar moieties and saponification occurs, which, in the case of the dyes considered here, results in acylation of the ANCs – typical of aliphatic acid acetylation.

Given the previously mentioned significant development in printing of edible vegetable dye inks on packaging paper and food substrates (Khan, et al., 2015; Fan, et al., 2019), clearly the preservation of coloration against pH degradation is already a topic of research. Similarly, as discussed here in this work, during drop-on-demand (DOD) inkjet printing on alkaline substrates partial ACN saponification may occur even if the eluted solution is immediately acidified (Dimić-Mišić, et al., 2015). In parallel, the use of natural dyes as photosensitisers is based on their large spectral absorption coefficients resulting in high light-harvesting efficiency, particularly in combination with TiO_2. Their natural renewable abundance, low cost and ease of preparation, whilst leaving no harm to the environment, means that their development in organic photoelectric devices is actively pursued, effectively eliminating concern of resource limitations.

In most of the cases introduced above, natural dyes' photoactivity is reliant on the presence of the ANC chemical family (Fan, et al., 2019; Mahmood, et al., 2018; Vandeput, 2021; Vatai, et al., 2008; Wathon, et al., 2019). However, when used as a dye in uncontrolled contact with a base there remains a major challenge, especially when faced by the ever-wider application of alkaline calcium carbonate. Natural dyes and calcium carbonate come into contact especially when the mineral is used as a filler in the food and paper industry, as well as in pharmaceuticals, mainly as functional excipient. This broad range of applications brings, newly, the concern in printing applications of anthocyanin-containing natural inks that they will exhibit discoloration. A strategy, therefore, is required to provide mitigation of this phenomenon, and to enhance the colour generation by application and substrate design. The work presented here illustrates the parameters at play during dye interaction with alkali substrate, so that such a strategy can be more reliably designed.

2. Material and methods

2.1 Aronia source, extract, and dye properties

Two different sources of Aronia fruit were used for investigating colour stability and printing. Aronia F (Northeast Finland) and Aronia L (Livonia – a historic region on the Eastern seaboard of the Baltic Sea in Latvia) with different compositions and colours (Figure 2). The extracts were obtained from clean fruits by crushing and dissolution using a pestle and mortar into a mixed solvent consisting of ethanol and water (1:1 in volume ratio). The samples were left at ambient temperature protected from exposure to direct sunlight to allow for adequate extraction of natural dyes in solution. It was found that consistent extract coloration was reached over a range of 3 to 5 days under these storage conditions. Solid residues were filtered out, and the clear solution was stored in a refrigerator at about +5 °C prior to printing (Velmurugan, et al., 2019).

Figure 2: Image of two different types of Aronia melanocarpa berries extract, at pH 3.3

2.2 Phenolic content measurement

Phenols, such as cyanidin-3-arabinoside, cyanidin-3-galactoside, (−)-epicatechin, chlorogenic and neochlorogenic acids, were analysed using high pressure liquid chromatography (HPLC). The stored methanolic extract from the Aronia was diluted by a factor of 100 with ACS (Attestation de Conformité Sanitaire: French attestation as potable) deionised water (supplied by Sigma-Aldrich, Merck Life Science OY, Keilaranta 6, 02150 Espoo, Finland) and filtered through a millipore

membrane filter (0.45 µm Nylon filter disk, Sigma-Aldrich). The HPLC apparatus (ESA Biosciences Inc., USA) consisted of a solvent delivery pump Model 582, guard cell Model 5010A (working electrode potential K1 = 600 mV, K2 = 650 mV), chromatographic column – Model Supelcosil LC8 (150.0 × 4.6 mm^2), 5 µm particle size and an electrochemical detector (Coulochem III). Chromatographic conditions were constant: 30 °C, mobile phase, being methanol and H^2O:H^3PO^4 = 99.5:0.5, (filtered through a filter Nylon, 0.2 µm, Sigma-Aldrich). The elution was isocratic, the flow rate of the mobile phase was 1.1 mL min^{-1} following the procedures as reported by Miki, et al., (1995) and Hwang, Sakakibara and Miki (1981). The content of phenols was calculated as mg kg^{-1} of fresh fruit mass.

2.3 Visualising the interaction with print substrate components

The interaction between the dye and substrate is primarily related to materials present in the substrate differing in pH from that of the acidic naturally occurring juice extract. Visualising the interaction is therefore undertaken using the individual component(s) responsible for the interaction both alone and in the composite structure of the substrate. Using this analytically designed approach allows us to deconvolute the material interactions from the multiple factors present in a ready-formed typical composite susbtrate.

2.3.1 Mineral pigment tablet forming method and UV-visible spectrophotometric method

Model single component substrates, consisting purely of mineral pigments as found in high brightness paper and board, were formed as compacted fine particle tablets made from water suspensions of titanium dioxide (TiO_2), and calcium carbonate ($CaCO_3$), respectively, each at the mass fraction 0.5 of mineral solids content. The TiO_2 pigment suspension supplied as powder from Sigma-Aldrich was produced by mixing deionised water into the dry powder using a high speed Diaf mixer for 30 min (Pilvad Diaf AS, Præstemosevej 2, 4, 3480 Fredensborg, Denmark). $CaCO_3$ was supplied as a coarse wet ground (GCC) marble-based product, Hydrocarb 60 (the mass fraction 0.6 of particles < 2 µm), in aqueous dispersion by Omya AG, Switzerland. The tablets were constructed by wet filtration through a fine 0.025 µm filter membrane under pressure (20 bar) in a steel die, according to a method developed by Ridgway, Schoelkopf and Gane (2003). The tablets were then dried overnight at 60 °C. After drying, the tablets were ground to remove scratches/surface defects occurring on the edges and surfaces by a flat grinder. The tablets were stored under standard testing conditions at 23 °C, and relative humidity, RH, 50 % for 24 h prior to dye absorption studies using the dye extract as ink. The optical properties of Aronia ink drops applied to tablets made from TiO_2 and $CaCO_3$ were assessed spectroscopically. Light transmittance and absorbance measurements were made using a UV-visible spectrophotometer (Shimadzu Model 160-A, Kyoto, Japan) across the wavelength range of 300–800 nm. Notably, differences in spectral response among the two constituent inks could be observed, which were primarily attributed to variation of refractive index contrast between each ink and the surrounding mineral in the tablets.

2.3.2 Change of pH effect arising from mineral pigment

Behaviour of Aronia dye as a function of mineral contact in combination with changing pH can be separated generally between low pH and mid-to-high pH conditions. At low pH, the potential for deprotonation of flavylium cations is suppressed, resulting in a lack of binding of ANC to flavylium cations, and possibly also preventing the binding of other dye components, due to charge repulsion. These changes can be induced by contact with mineral pigments (Asbury, et al., 2003). For example, when used in photosensitisers incorporating TiO_2 it was shown in solar cell application that lower observed short circuit photocurrent, $_{JSC}$, at basic pH may be explained by two different factors (Imanishi, et al., 2007). One of these is due to the decreasing driving force for electron injection caused by the upward shift of the conduction band edge of TiO_2 with increasing pH when used on printing paper and board, sometimes also containing some TiO_2, where the majority mineral is $CaCO_3$ alone (Asbury, et al., 2003; Imanishi, et al., 2007). This supports that contact with $CaCO_3$ mineral pigment results naturally in a rise of pH.

The natural pH was found to be 3.3 for Aronia F and 3.7 for Aronia L, similar to values reported by Skupien, Ochmian and Grajkowski (2008). Change in pH as a function of 0.1 M NaOH addition was monitored using a pH meter (SP-701, Suntex Instruments Co. Ltd., Kangning St., Xizhi Dist., New Taipei City, Taiwan). In addition to the impact of pH on dye properties, contact between acidic species and $CaCO_3$ results in the release of calcium ion, Ca_2+, which, in turn, can lead to coagulates forming with, and saponification of, the dyestuff. The effect of Ca_2^+ on ANC extract was studied by adding 3 M $CaCl_2$ to the samples of Aronia dye and measuring particle size development.

The coupled phenomena of pH change of Aronia inks, due to exposure to Ca_2^+ ions on contact with $CaCO_3$, and the resulting potential impact on coloration and colour fastness (stability of colour) are thus studied using the model substrates consisting of mineral pigment alone.

2.4 Inkjet printing process

In this study we used a lab scale DOD piezoelectric based inkjet printer, Fujifilm Dimatix material printer

DMP-2831 (Fujifilm Corp., Midtown, Akasaka, Minato, Tokyo, Japan) using the manufacturer's DMC-11610 ink cartridges with nominal 10 pL drop volume to realise a proof-of-concept study (Koivunen, Jutila and Gane, 2015; Dimić-Mišić, et al., 2015). Droplet jetting frequency of 1 kHz was applied to all the ink extracts and to evaluate uniformity and optical properties of printouts of the dye samples. Printing was performed at room temperature (23 °C).

2.5 Characterisation of printouts

Printing papers were provided by Stora Enso (Lumi - Press, 170 g/m^2 substance and 0.7 µm roughness). The information about uniformity and surface morphology of printed electrolyte patterns was determined with optical light microscope (Leica Microsystems).

2.6 Rheological Tests

Since inkjet printing, being one of the most likely technologies to be used, subjects ink to various flow conditions during pumping, ejecting, drop splitting and substrate surface flow it is important to evaluate its resistance to these applications of shear and strain, and of particular interest is the change of these properties over time in response to physical and chemical interactions.

Rotational instrumentation is commonly used to study the rheological response of liquids and colloidal suspensions to shear, depending on the rotation rate and gap between the elements defining the physical experimental boundaries. Parallel plate–plate confinement is one such typical liquid geometry, where, in this case, the sample was loaded onto the lower of the two parallel plates of a Physica MCR 301 rheometer, (Anton Paar, Graz, Austria), and the upper plate then lowered until the distance between the two plates was 0.5 mm. Temperature throughout the measurement was held at 23 °C, and an anti-evaporation cover was attached onto the rheometer upper plate to minimise measurement errors arising from the loss of solvent (water evaporation) during the experiment. The inks were initially subjected to a pre-shearing shear rate ($\dot{\gamma}$) of 50 s^{-1} for 30 s, and left to rest stationary for 60 s. Shear rate ($\dot{\gamma}$) input values were ranged between 0.01 and 1 000 s^{-1} to study the dynamic viscosity response (η) of the inks. Response of the dye solution to shear rate is critical during expulsion from the inkjet printer nozzle and in respect to flow on the substrate surface and absorption rate into pores, if present.

By applying controlled strain using electronic feedback, the derived internal stress in the sample can be determined (Duffy, et al., 2015). This method, without resorting to oscillation, is useful for retaining materials in suspension, where otherwise there might be sedimentation (Dimić-Mišić, et al., 2015; Mahmood, et al., 2018; Medina-Meza, et al., 2016). The stress response of the Aronia dye solutions is important both at the impulse time of pressure application to initiate droplet formation and upon impact with the substrate surface.

2.7 FTIR analysis

In the interests of understanding changes in chemical composition of the dyes as a function of pH, Ca_2+ exposure and physical shear samples were analysed using Fourier transform infra-red (FTIR) spectroscopy (Perkin Elmer, Revvity Finland OY, Mustionkatu 6, 20750 Turku, Finland) before and after shearing by forming dried ink films. The films were made by pouring a thin layer of suspension in a Petri dish and then drying at room temperature (23 °C), whilst protecting from direct light.

2.8 Particle size measurements

Size data were reported as particle diameter derived from time-averaged static light scattering as a function of scattering angle from a dilute dispersed suspension of particles using a Malvern Instruments Mastersizer (Malvern Pananalytic 3000 Ltd., Malvern WR14 1XZ, UK). The particle size distribution is represented by the volume of particles present having a size less than a given size, d_{SV}, e.g., the median volume based particle size is represented by the diameter of the particle for which the volume fraction 0.5 of particles are finer than d50 %.

3. Results and discussion

3.1 Phenolic content of Aronia extracts

The phenolic content, present in different amounts in the two geographically separate samples of Aronia melanocarpa, Aronia F (sourced from Finland) and Aronia L (sourced from Latvia), together with their chemical element analysis are presented in Table 1 and Table 2, respectively.

Both Aronia melanicarpa samples were rich in minerals, which relate to their well-known trace element nutraceutical properties and their antioxidant action (Kampuse, et al., 2009; Sarv, et al., 2021; Angelova, et al., 2017), with Aronia F ink having somewhat higher levels of Al, Na and K ions, Table 2.

3.2 Effect of pH and link to print application on modern $CaCO_3$ coated paper

As depicted in the Figure 3, the colour of the Aronia extract, as predicted, undergoes discernible changes with fluctuations in pH content. The observed variations highlight the pH-dependent nature of the extract, showcasing a dynamic interplay between pH levels

Table 1: The most important constituents of Aronia melanocarpa extracts TPC = total phenolic content, TPAC = total phenolic acid content, TAC = total anthocyanin content is seen to differ in amount between Aronia F and Aronia L

Phenolic type and content in sample extract	Aronia F	Aronia L
TPC (mg GAL L^{-3})	12 857 ± 200	77 816 ± 106
TPAC (mg GAL L^{-3})	919 ± 116	589 ± 96
TAC (mg Gy-3 GalE L^{-3})	13 233 ± 167	8 312 ± 143

and the resultant coloration, as with increasing pH colour changes from purple to red then towards blue and greenish yellow. Figure 3a) illustrates the colour change as a function of pH controlled by addition of NaOH, as exemplified in the case of Aronia F ink extract.

By viewing the spreading of ~ 0.1 mL droplets of ink at each pre-adjusted pH level placed on calcium carbonate coated paper Figure 3b) reveals the formation of particulate material in the ink-on paper state starting at pH value 3.3 and extending to 8.7. However, less particulate matter is produced when the ink is applied at pH 10.4, and the consistency of dye coloration (yellow) is the purest of the series by being essentially free from particulates except for the image edges. The Marangoni effect, often referred to as the coffee stain effect, is clearly demonstrated here, whereby the progressively concentrating ink dye is transported, as a function of absorption into the porous coating and drying time, toward the droplet spread perimeter. This transport phenomenon also concentrates the coagulate particles formed in the presence of Ca^{2+}, being released from the $CaCO_3$ coating pigment. Additionally, colour dye component separation is clearly observable suggesting that a chromatographic process of adsorption to the $CaCO_3$ coating pigment particle surface may also be at play. Figure 3c) in turn demonstrates how the microscopic spread of printed inkjet dots eventually begins to lead to the desired full tone image on the paper surface.

3.3 Additional impact of exposure to Ca^{2+}

To illustrate the result arising from extended exposure of acidic Aronia dye inks to $CaCO_3$ typically found in modern papers as filler coating pigment, and suspected to have caused coagulation as seen previously in Figure 3, the ink extracts were mixed, respectively, with the $CaCO_3$ pigment suspension with the mass fraction 0.5 as was used as precursor to forming the mineral tablets (studied further in the section 3.6). The high brightness of the $CaCO_3$ suspension clearly dominates the colour of the mix, as shown in Figure 4 b) before and after Aronia L ink addition, but the ink nonetheless provided an observable tinge of col-

Table 2: The chemical element analysis of elements present in the sample extracts of Aronia melanocarpa

Mineralic element	Ion content /mg L^{-1}	
	Aronia F	Aronia L
Al	121.1	95.7
Fe	23.9	22.9
Mn	13.6	25.1
Mg	954.4	963.3
Ca	1449.1	1729.7
Na	233.4	129.4
K	11 601.5	9306.3

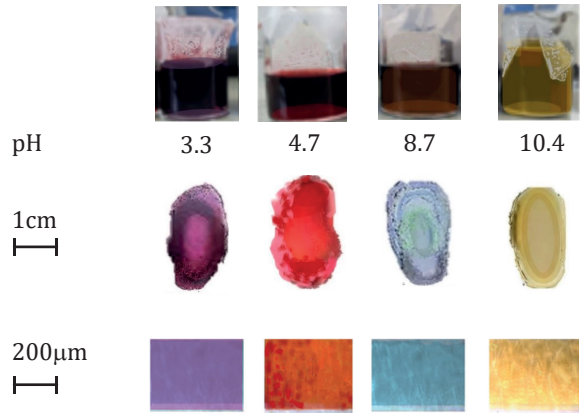

Figure 3: Appearance of Aronia F ink at room temperature: a) change of pH in alcohol ink extracts causing change in colour, b) spreading of macroscopic ink droplets on contact with $CaCO_3$ coated paper substrate and c) optical micrographs of inkjet printed dots on paper showing their merging to form a solid full tone image by ink dot spreading

oration to the eye. The mixed samples were placed for 24 h in refrigerated storage at 5 °C. Following this storage time, it was observed that a pink foam layer had formed in the neck of the glass storage vials. The foam product is illustrated in Figure 4 c), where the comparative colour is just discernible between the remaining bulk of the mixed suspension and the extracted foam-including layer. These effects reflect the combined impact of raised pH to that of naturally occurring $CaCO_3$ acting as buffer and the exposure to Ca^{2+} resulting from the acid-base reaction. In addition, it was seen that the amount of foam, indicating acidic reactivity, was greater for the Aronia F versus Aronia L, which is in accordance with the higher acidic phenolic content in Aronia F.

To analyse further the chemical product arising from Ca^{2+} reactivity alone the ink samples were treated by the addition of $CaCl_2$, and the difference in reactivity between the inks, related to Ca^{2+} without excess base

present, was observed. In this case, contrary to when base is present, and in accordance with phenolic acid content, Table 1, ink in which ANC and phenols (TPC, TAC, TPAC) were less prevalent, and, hence, required less ionic exchange to coagulate, reacted faster and produced greater thickening with aging (Fan, et al., 2019; Khoo, et al., 2017; Vandeput, 2012). FTIR analysis revealed the suspected presence of additional species constituting calcium soap particles, Figure 4 a).

Formation of coagulates upon $CaCl_2$ addition was studied via monitoring the increase in particle size within the ink suspension. Figure 5 shows how the median particle size increases significantly when the ink was exposed to Ca^{2+} ion, rising from a value ~ 60 µm to 68 µm and 72 µm, respectively, for Aronia F and Aronia L. Although this increase in median particle size might not in itself impact inkjet printing jettability, the real problem lies in the extension at the coarse end of the particle size distribution, where particles as large as 85–90 µm, which were not present in the original ink, not only appear, but have significant random occurrence, shown by the rise in the curve (insert in Figure 5) at this large particle size, particularly in the case of Aronia L. Of note also is the formation of a shoulder representing increased fine particles upon exposure to Ca^{2+}, seen as a shoulder to the left of the size distribution curves, Figure 5, for both inks. In the case of Aronia F the increase in fines ranges from around 38 to 53 µm, whereas that for Aronia L displays ultrafine particles generated over an even greater extended range from 25 to 50 µm. This suggests that the process includes not only a coagulating Ca^{2+} bridging effect between acid groups of existing particles, leading to coarser particulates, but a seeding of fine insoluble salt particles arising from calcification of soluble acidic ink species.

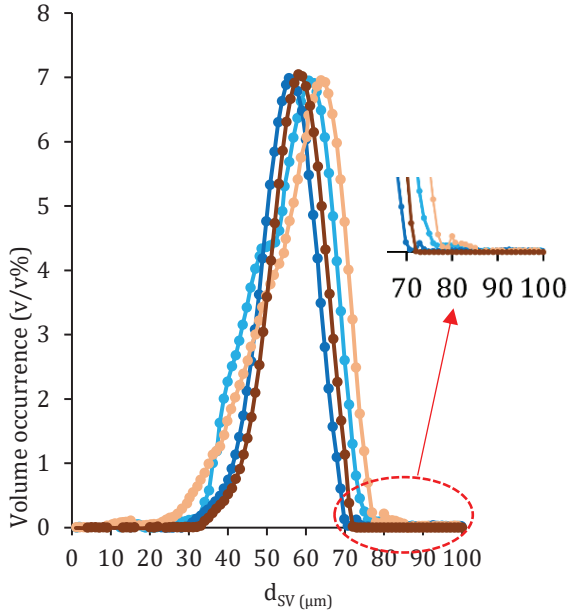

Figure 5: Particle size distributions for the two Aronia inks F and L, comparing before and after the addition of $CaCl_2$, showing both formation of fine insoluble salt particles and the coagulation of existing particulate matter to form significantly larger particles

3.4 Rheological effect of pH on ink stability

Controlling the viscoelastic behaviour of the inks is crucial for the jetting performance of the droplets in inkjet printing applications (Medina-Meza,, et al., 2016). Although in many inkjet printing studies only zero-shear rate viscosity of the inks has been presented for the initial jetting flow characteristics of the printing inks, based on the assumption of Newtonian behaviour, more measurement points need to be added into

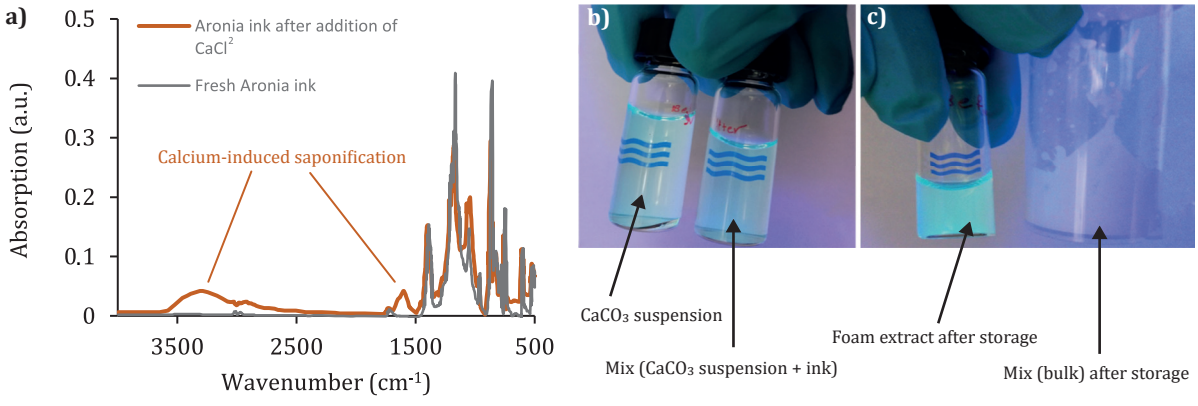

Figure 4: a) FTIR spectra showing difference in molecular structure as a result of saponification and particle formation in Aronia ink extract upon addition of $CaCl_2$ before and after storage, b) mixing Aronia L ink with $CaCO_3$ suspension and c) separating the upper layer of foam from stored sample mix of $CaCO_3$ and Aronia F

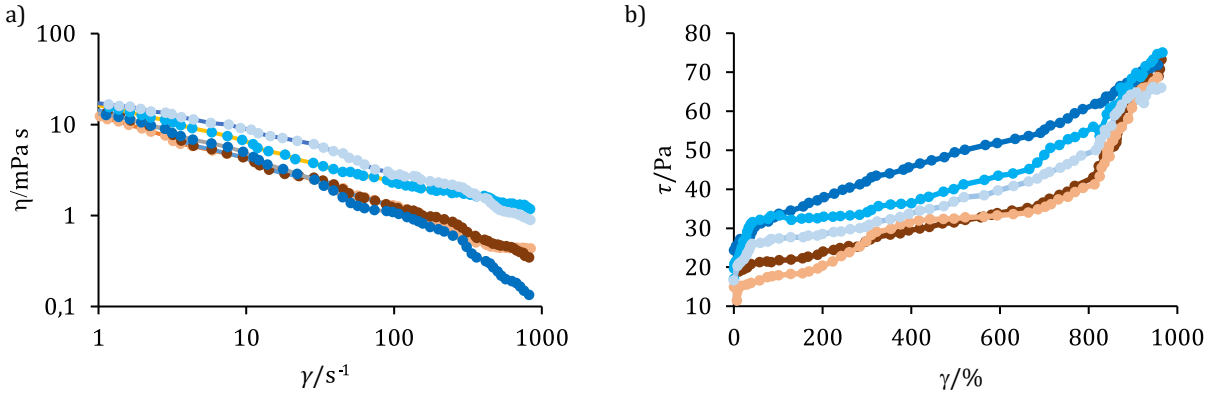

Figure 6: Steady state response of Aronia inks, a) dynamic viscosity over the range of shear rate, and b) static stress response to strain

the experiments in the case of non-Newtonian fluids (Dimić-Mišić, et al., 2015; Hashmi, et al., 2015). Dynamic viscosity measurements of the liquids indicated a shear thinning behaviour at low to medium shear rates, and thickening behaviour (dilatancy) at higher shear rates for those samples, suspected of containing concentrated particles in suspension (Dimić-Mišić, et al., 2015; Mahmood, et al., 2018). When considering inkjet nozzle function, dilatant behaviour is undesirable as it can result in clogging of nozzles, which directly disturbs printing performance (Mahmood, et al., 2018; Medina-Meza, Boioli and Barbosa-Cánovas, 2016). The greatest rheological stability was observed for inks at their natural pH, in acidic condition, with continuing shear thinning at the higher shear rates, Figure 6a). However, at the higher shear rates measured, the energy release is reflected in a strong growth of internal stress response to high levels of strain, Figure 6b). In contrast, inks adjusted to higher pH levels showed initial stress increase from the stationary state, but then did not dissipate excess energy at the highest strain levels, Figure 5b), displaying a monotonic stress behaviour upon increase in alkalinity.

Moreover, it is noteworthy to mention that the agglomeration phenomenon in the suspension would, once again, have practical implications, particularly in the context of formulation and manufacturing processes. The size and distribution of aggregates can affect the rheological properties, stability, and quality of the Aronia based products, such that inkjet printing would no longer be reliable in respect to jettability. Thus, considering pretreatment with Ca^{2+} ion cannot be considered as viable for inkjet printing, and so was not analysed rheometrically in this study.

3.5 UV-Vis absorption spectra and optical effect on mineral coating pigment

The dye optical properties of the Aronia inks were evaluated using spectrophotometry across the ultraviolet (UV) and visible (Vis) light spectrum. Dyes deliver coloration by absorbing the complementary colours in the visible spectrum, thus transmitting light having the characteristic colour band of the dye only. Figure 7, a) and b), shows the optical absorbance and transmittance spectra, respectively, for the Aronia F and Aronia L inks across the wavelength range 300–800 nm.

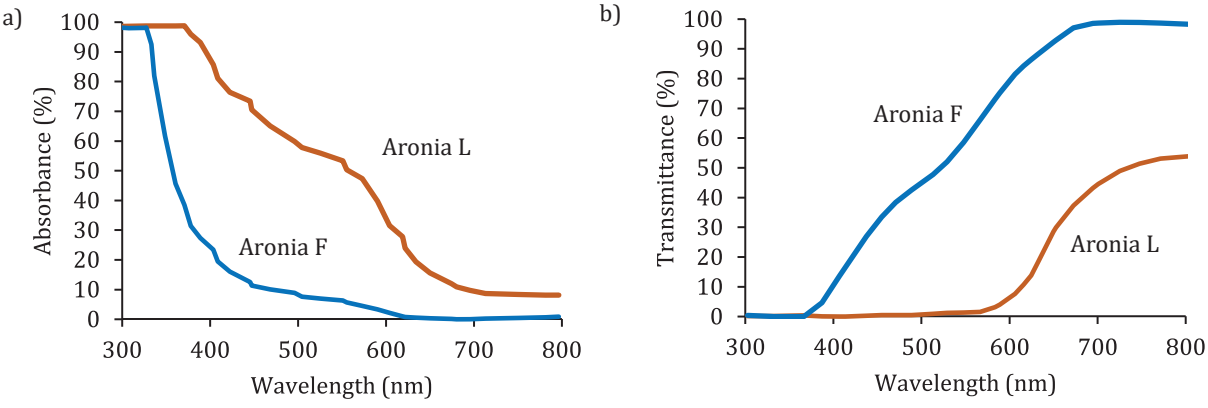

Figure 7: Optical spectral properties of Aronia F and Aronia L dye extract inks, a) light absorbance, and b) light transmittance depending on the ratio of anthocyanin and total phenolic content of the inks Aronia F and Aronia L (Table 1)

Comparing the light filtration properties of the dyes, the spectrometric absorbance and transmittance as a function of wavelength determine both the colour spectral response and the intensity or purity of the inherent dye coloration. Considering the spectra shown in Figure 7, a) and b), it is clearly possible to discern the distinct difference in breadth of the spectral response. The Aronia F dye contains more ANC and phenolic compounds (PC) in total, resulting in a more specifically active absorption at short wavelength compared with the broad spectrum absorbing Aronia L dye (Vandeput, 2021; Vatai, et al., 2008; Borowska, et al., 2020). These differences lead to the coloration print density reflectance properties of the combined system of dye on and penetrated within a porous substrate.

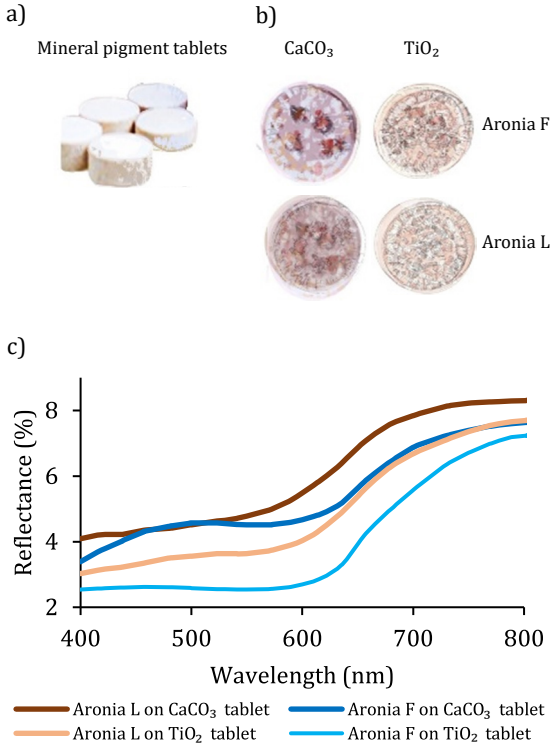

Figure 8: a) Porous tablets formed from $CaCO_3$ and TiO_2 each at the mass fraction 0.5 of pigments in water suspension, b) images of ink droplets applied to the surface of $CaCO_3$ and TiO_2 based tablets (note the greater colour intensity for ink on $CaCO_3$ compared with TiO_2, c) diffuse spectral reflectance measured from the dye impregnated tablet area

Drops of Aronia F and Aronia L inks were put onto the surface of the $CaCO_3$ and TiO_2 compression formed tablets (Figure 8a), respectively, and the ink in each case was clearly seen to be absorbed via capillary imbibition. Due to the necessarily higher porosity of the coarser particle size $CaCO_3$, volume penetration within the $CaCO_3$ tablet was more rapid. In both material cases, the colours of the tablets changed in response to the presence of the dye, with reactivity and change in pH being greater in the case of $CaCO_3$, as was expected (Figure 8b). Additionally, the points of applied ink on the $CaCO_3$ tablet appeared more intense on the $CaCO_3$ than on the TiO_2 tablet, even though ink penetration was faster for $CaCO_3$. This observation is important when considering the dye colour intensity desired for a given print, i.e. less ink is required when printed on the $CaCO_3$ to achieve the same print density. Upon comparison, the refractive index of $CaCO_3$ is typically ~1.51 whereas that of TiO_2 in the rutile form is almost double at 2.87, with a virtually complete light absorption at a wavelength of 632.8 nm having a transmission coefficient of 0.

The observed print density phenomena, relating to the coating material and structure, for a dye ink print predominantly centre on a combination of porous matrix light scattering, related to optimal pore size and pore occurrence at that size, versus surface light scattering and absorption as a function of high material refractive index. Thus, high light scattering from optimally sized pores (~ 0.2 µm for visible light) containing dye held within a matrix of bright low light absorbing $CaCO_3$ particles results in a greater amount of dye-filtered light returning to an external observer than the case where highly light absorbing TiO_2 masks the internal volume of the coating layer preventing light from entering the interparticle pores deeper in the porous matrix. Furthermore, the intense light back-scattered from the TiO_2 surface particle layer reduces the colour contrast even further due to high white light content returning to the external observer. This balance of contrasting light scattering properties of the porous substrate, combined with accessible dye performing light spectral filtration determines the coloration and intensity as measured by the spectrometer operating in diffuse reflection mode, Figure 8c). Interpreting the reflectance to define coloration intensity requires the observer to note the sharpness of specificity change in diffuse reflectance across the wavelength spectrum studied. A pure intense coloration is seen when the reflectance is low across much of the spectral range but rises sharply over one or more narrower spectral band(s), typical of the dye colour itself. Thus, studying the reflectance curve of Aronia F applied onto the $CaCO_3$ tablet in comparison to the others, reveals distinct specificity both at medium to short wavelength and at long wavelength, which well describes the strong purple-to-red nature of the colorant. The broader reflectance curves for Aronia L well represent its less specific coloration, being reddish brown in nature.

4. Discussion

ANCs, when extracted, exhibit lower stability compared to when held within the intact berry structure. Once

isolated, ANCs are prone to degradation or change influenced by environmental factors like pH and ionic content in suspension, and temperature and light exposure, ultimately diminishing both their health-promoting attributes and colorant applications.

Aronia L particles were larger than those of Aronia F, and for both types of Aronia an increase of diameter is seen with addition of Ca^{2+} ions due to the possibility of coagulation between ANCs and pectin and Ca^{2+} ion at lower pH (Borowska, et al., 2020; Fu, et al., 2023). The presence of Ca^{2+} ions has been observed to exert a significant impact on the pH level of Aronia extract due to the neutralising effect of calcium salt production, consequently influencing the agglomeration dynamics within the suspension. This phenomenon plays a crucial role in moderating both the amount of flocculation and the size of agglomerated coagulates within the system. In general, increase in pH is likely to alter the surface charge of particles in the Aronia extract, leading to modifications in their colloidal behaviour due to the resulting effects on the electrostatic and van der Waals forces governing particle interactions, thereby influencing the agglomeration state of the suspension.

A comparative analysis of the reflectance changes between tablets fabricated from calcium carbonate ($CaCO_3$) and those composed of rutile titanium dioxide (TiO_2) reveals intriguing insights. The variations in reflectance can be indicative of differences in the optical properties, surface characteristics, or composition of the two types of tablets. On the one hand, the tablets made from $CaCO_3$ may exhibit distinct reflectance patterns, potentially associated with the birefringent interaction of light with the crystalline structure of calcite, a property not studied within the scope of this current work. On the other hand, tablets consisting of TiO_2 might display different interactive dye reflectance profiles across the pH related changes in dye coloration due to the unique photon exchange optical properties of titanium dioxide (Błaszczyk, et al., 2021; Zhang, et al., 2023). The effect of pH could, therefore, indicate a difference in solar cell performance if used in such photosensitising applications, in respect to shift in colour spectrum from purple to red, for low pH of 4.7, towards blue, at 7.4, and yellow at 10.4 (Woo, et al., 2021). Similarly, current density would likely be affected, depending on amount of molecular constitution changes (Fan, et al., 2019; Khan, et al., 2015; Wathon, et al., 2019). Further study understanding these reflectance changes would provide valuable information for applications such as pharmaceutical tablet identification and product encoding, quality control, and the assessment of material characteristics (Fu, et al., 2023; Liu, Fang and Ng, 2023).

Considering the diffuse reflectivity behaviour resulting from dye–substrate structure interaction in combination with the spectral changes undergoing by the dye as a function of pH and Ca^{2+} exposure, it is clear that printing acidic natural plant dye inks onto modern alkaline substrates is challenging, not only in respect to long time colour fastness, but also in respect to colour gamut and photocatalytic effects.

4.1 Proposal of how to cope with the challenges

Resulting from the work presented in this paper, we undertake to make a short series of process proposals, which could be useful to the industry when attempting to fulfil the growing demand for the use of printing inks derived from natural plant dyes, especially when considering inkjet printing.

(i) Control pH of the ink in advance by a dilute base, simultaneously carefully analysing the spectral properties of the ink at pH ~ 8.8 as defining the end point coloration.

(ii) Promote rapid ink drying on $CaCO_3$ containing papers to prevent excessive saponification and ink particle coagulation. To achieve this, adopt highly porous coatings with strong capillarity, i.e. promote the presence of ultrafine pores.

(iii) Preferably use small volumes of ink, spatially densely applied. This latter requires increased jetting frequency to provide full tone areas through printed dot merging prior to rapid drying.

(iv) Adopt a strategy to buffer the $CaCO_3$, rendering it acid tolerant by capturing Ca^{2+} released during acid interaction, thus maintaining the surrounding ambient acid pH of the ink. This is known to be achievable by combining the chelating action of reactive species, such as polyacrylate and/or polyamide groups with a weak base, such as considered in (i) above. The effect will be enhanced naturally by the weak to medium strong acidic properties of the dye itself, following the principle described by Wu (1997). Such a chelating agent in combination with the conjugate base could be used as part of the acid ink formulation. Testing this approach is, therefore, a subject for further work.

The main advantages of investing in natural ink dye products for functional printing of, for example, electronics and photosensitive energy production and storage devices are the low cost of the technology, the potential to recover device components and recycle the substrate as well as the active materials, following circular economy precepts, and rendering the product environmentally harmless whilst promoting biocompatible and naturally degradable devices (Okello, et al., 2022). Open Sound Control (OSC) as protocol for data transport specification and encoding during real-time

message communication among applications and hardware or electronic paper are already becoming commercially demanded products. Prototypes of devices like paper batteries, solar cells, nanopaper transistors, thermoelectric nanogenerators, graphene-enabled optoelectronics, biosensors, and even microfluidic lab-on-chip devices are under ongoing development. In these applications, paper can be used simply as the flexible substrate onto which researchers transfer thin-films, nanoparticles, or other nanostructures via various processes such as printing.

The value of considering pH sensitive dyes as sensors for a range of applications has already been recognised, especially, as mentioned earlier, when considering storage stability of perishable materials (Singh, Gaikwad and Lee, 2018). However, inverting the argument of coloration sensitivity from sensor to image reproduction results in a fascinating opportunity. As shown here, ANC dye can adopt a wide range of colours depending on its chemical and physical surrounding matrix (porous substrate) properties. The range closely approximates the standard cyan–magenta–yellow (CMY) component criteria for CMYK four colour printing. Deficiency in precise colour summation might be correctable by addition of further dyestuff to achieve full colour gamut.

Alternatively, if a method could be found to fix the dye to a substrate component(s), or component in solution, in such a way that the sensitivity of coloration to further chemical environmental change is suppressed, the hypothesis of covering the colour gamut with a single green-chemistry source could lead to a fully sustainable, biodegradable printing ink set structure.

A further alternative to chemically fixing the dye, and even more novel, could be to print a single pH sensitive dye at all pixel dots of an image. Then, virtually simultaneously, in alignment print the suitable activating pH-defined buffer as a secondary ink to generate in-situ the necessary coloured pixel. Each buffer could be selected from the complementing pH range needed to be applied to generate the respective dye response colours. In this way, the complete desired coloured image could be generated.

5. Conclusions

It is especially in the field of functional printing on modern available substrates where the challenges arise applying acidic plant dye ink onto porous alkaline filled or coated substrate. Understanding the interactions at play can enable the practitioner to predict and counter undesirable effects affecting process choice and runnability, economics, end product quality and its place in circular economy with focus on minimising or eliminating environmental impact. Following procedures such as those demonstrated in this current study can provide a framework for building the necessary control mechanisms to ensure application success. The result being, as hereby illustrated, that a simple action flowchart of checks and analyses can be generated for specific cases, and necessarily implemented under a policy of continuous process improvement to meet the emerging challenges within the functional print industry. Opportunities for applying natural plant dye inks are continuing to grow, and exploration of their interactions with environmental factors effecting and affecting the functionality of printed devices will remain a fertile area for further development. We can thus conclude that, in accordance with the title of this paper – 'natural plant dye inks set new challenges' – the opportunity to extend the boundaries of these challenges remains an exciting prospect for novel technology, not only supporting already identified applications but even considering full colour imaging from a single, or complementary, plant dye by post adjustment of pH and fixation. Such opportunities also extend to other photo-functionalities.

References

Angelova, V.R., Tabakov, S.G., Peltekov, A.B. and Ivanov, K.I., 2017. The effect of soil contamination on chemical composition and quality of aronia (Aronia melanocarpa). *International Journal of Agricultural and Biological Engineering*, 11(11), pp. 787–792.

Arya, P., Wu, Y., Wang, F., Wang, Z., Marques, G. C., Levkin, P. A., Nestler, B. and Aghassi-Hagmann, J., 2024. Wetting behavior of inkjet-printed electronic inks on patterned substrates. *Langmuir*, 40, pp. 5162–5173: https://doi.org/10.1021/acs.langmuir.3c03297.

Asbury, J. B., Anderson, N. A., Hao, E., Ai, X. and Lian T., 2003. Parameters affecting electron injection dynamics from ruthenium dyes to titanium dioxide nanocrystalline thin film. *The Journal of Physical Chemistry B*, 107(30), pp. 7376–7386. https://doi.org/10.1021/JP034148R.

Błaszczyk, A., Joachimiak-Lechman, K., Sady, S., Tański, T., Szindler, M. and Drygała, A., 2021. Environmental performance of dye-sensitized solar cells based on natural dyes. *Solar Energy*, 2(215), pp. 346–355. https://doi.org/10.1016/j.solener.2020.12.040.

Borowska, S., Tomczyk, M., Strawa, J. W. and Brzóska, M. M., 2020. Estimation of the chelating ability of an extract from Aronia melanocarpa L. Berries and its main polyphenolic ingredients towards ions of zinc and copper. *Molecules*, 25(7):1507. https://doi.org/10.3390/molecules25071507.

Cotabarren, I. M., Cruces, S. and Palla, C. A., 2019. Extrusion 3D printing of nutraceutical oral dosage forms formulated with monoglycerides oleogels and phytosterols mixtures. *Food Research International*, 126, pp. 108676–108687. https://doi.org/10.1016/j.foodres.2019.108676.

Dangles, O., Saito, N. and Brouillard, R., 1993. Anthocyanin intramolecular copigment effect. *Phytochemistry*, 34(1), pp. 119–124. https://doi.org/10.1016/S0031-9422(00)90792-1.

Dimić-Mišić, K., Karakoc, A., Ozkan, M., Hashmi, S. G., Maloney, T. and Paltakari, J., 2015. Flow characteristics of ink-jet inks used for functional printing. *Organic Electronics*, 38, pp. 307–315. https://doi.org/10.1016/j.orgel.2016.09.001.

Duffy, J. J., Hill, A. J. and Murphy, S. H., 2015. Simple method for determining stress and strain constants for non-standard measuring systems on a rotational rheometer. *Applied Rheology*, 25(4), pp. 8–13. https://doi.org/10.3933/applrheol-25-42670.

Fan, H., Zhang, M., Liu, Z. and Ye, Y., 2019. Effect of microwave-salt synergetic pre-treatment on the 3D printing performance of SPI-strawberry ink system. *LWT*, 122:109004. https://doi.org/10.1016/j.lwt.2019.109004.

Fu, W., Li, S., Helmick, H., Hamaker, B. R., Kokini, J. L. and Reddivari, L., 2023. Complexation with polysaccharides enhances the stability of isolated ANCs. *Foods*, 12(9):1846. https://doi.org/10.3390/foods12091846.

Gane, P.A.C. and Koivunen, K., 2010. Relating liquid location as a function of contact time within a porous coating structure to optical reflectance. *Transport in Porous Media*, 84, pp. 587–603. https://doi.org/10.1007/s11242-009-9523-x.

Gane, P.A., Imani, M., Dimić-Mišić, K., and Kerner, E., 2021. Novel device for determining the effect of jetting shear on the stability of inkjet ink. *Journal of Print and Media Technology Research*, 10(1), 7–24. https://doi.org/10.14622/JPMTR-2015.

Hakim, L., Deshmukh, R.K., Lee, Y.S. and Gaikwad, K.K., 2024. Edible ink for food printing and packaging applications: a review. *Sustainable Food Technology*, 2, pp. 876–892. https://doi.org/10.1039/d4fb00036f.

Hashmi, S.G., Ozkan, M., Halme, J., Dimic Misic, K., Zakeeruddin, S.M., Paltakari, J., Grätzel, M. and Lund, P.D., 2015. High performance dye-sensitized solar cells with inkjet printed ionic liquid electrolyte. *Nano Energy*, 17, pp. 206–215. https://doi.org/10.1016/j.nanoen.2015.08.019.

Hellström, J.K., Shikov, A.N., Makarova, M.N., Pihlanto, A.M., Pozharitskaya, O.N., Ryhänen, E–L., Kivijärvi, P., Makarov, V.G. and Mattila, P.H., 2010. Blood pressure-lowering properties of chokeberry (Aronia mitchurinii, var. Viking). *Journal of Functional Foods*, 2(2), pp. 163–169. https://doi.org/10.1016/j.jff.2010.04.004.

Henneberg, M. and Stasrznewicz, M., 1993. Herbal ethnopharmacology of Lithuania/Vilnius region III: Medicament and Food. In: *Actes du 2e Colloque Européen d'Ethnopharmacologie et de la Conférence Internationale d'Ethnomédecine*, Heidelberg, 1993. Paris: IRD Éditions, pp. 243–255.

Huang, S., Basore, P., Boyd, M., Jones-Albertus, B., Nilsen, G., Silverman, T., Sodano, D. and Tinker, L., 2022. *Solar Energy Technologies Office Photovoltaics End-of-Life Action Plan*. US Department of Energy, Office of Energy Efficiency and Renewable Energy, DOE/EE-2571: energy.gov/eere/solar.

Huang, R. and Xu, C. (2023). Sensory property and phenolic profile of aronia juice. In: Mérillon, JM., Riviere, C., Lefèvre, G. (eds) *Natural Products in Beverages*. Reference Series in Phytochemistry. Springer, Cham. https://doi.org/10.1007/978-3-031-04195-2_73-1.

Hwang, B. H., Sakakibara, A. and Miki, K., 1981. Hydrogenolysis of Protolignin-XVII. Isolation of three dimeric compounds with y–0–4, ß–1, and ß–0–4 linkages from hardwood lignin. *Holzforschung*, 35(5), pp. 229–232. https://doi.org/10.1515/hfsg.1981.35.5.229.

Imanishi, A., Okamura, T., Ohashi, N., Nakamura, R. and Nakato, Y., 2007. Mechanism of water photooxidation reaction at atomically flat TiO_2 (rutile) (110) and (100) surfaces: dependence on solution pH. *Journal of the American Chemical Society*, 129(37), pp. 11569–11578. https://doi.org/10.1021/ja073206.

Jurič, I., Karlović, I., Tomić, I. and Novaković, D., 2013. Optical paper properties and their influence on colour reproduction and perceived print quality. *Nordic Pulp & Paper Research Journal*, 28(2), pp. 264–273. https://doi.org/10.3183/npprj-2013-28-02-p264-273.

Kampuse, S., Krūma, Z., Kampuss, K. and Krasnova, I., 2009. Nutritional value of minor fruits in Latvia. *Acta Horticulturae*, 877: pp. 1221–1228. https://doi.org/10.17660/ActaHortic.2010.877.166.

Khan, M.Z., Al–Mamun, M.R., Al-Amin, M., Moniruzzaman, M. and Hasan, M.R., 2015. Dye-sensitized solar cell using used semiconductor glass and natural dye: towards alternative energy challenge. *International Journal of Renewable Energy*, 5(2), pp. 38–44.

Khoo, H.E., Azlan, A., Tang, S.T. and Lim, S.M., 2017. Anthocyanidins and ANCs: Colored pigments as food, pharmaceutical ingredients, and the potential health benefits. *Food & Nutrition Research*, 61(1):1361779. https://doi.org/10.1080/16546628.2017.1361779.

Koivunen, K. and Gane, P.A.C., 2010. Optical reflectance as a function of liquid contact time and penetration depth distribution in coatings with mono and discretely bimodal pore size distributions, *Proceedings of the 2010 TAPPI Advanced Coating Fundamentals Symposium*, TAPPI Press, Atlanta GA, pp. 108–128.

Koivunen, R., Jutila, E. and Gane, P., 2015. Inkjet printed hydrophobic microfluidic channelling on porous substrates. *Journal of Print and Media Technology Research*, 4(1), pp. 7–17. https://doi.org/10.14622/JPMTR-1413.

Leonard, P.J., Brand, M.H., Connolly, B.A. and Obae, S.G., 2013. Investigation of the origin of Aronia mitschurinii using amplified fragment length polymorphism analysis. *Hort. Science*, 48(5), pp. 520–524. https://doi.org/10.21273/HORTSCI.48.5.520.

Liu, S., Fang, Z. and Ng, K., 2023. Recent development in fabrication and evaluation of phenolic-dietary fiber composites for potential treatment of colonic diseases. *Critical Reviews in Food Science and Nutrition*, 63(24), pp. 6860–6884. https://doi.org/10.1080/10408398.2022.2043236.

Mahmood, K., Alamri, M. S., Abdellatif, M. A., Hussain, S., Qasem, A. A., 2018. Wheat flour and gum cordia composite system: Pasting, rheology and texture studies. *Food Science Technology*, 38, pp. 691–697. https://doi.org/10.1590/FST.10717.

Mary, S.K., Koshy, R.R., Daniel, J., Koshy, J.T., Pothen, L.A. and Thomas, S., 2020. Development of starch based intelligent films by incorporating ANCs of butterfly pea flower and TiO_2 and their applicability as freshness sensors for prawns during storage. *RSC Advances*, 10(65), pp. 39822–39830. https://doi.org/10.1039/d0ra05986b.

McKay, S.A., 2001. Demand increasing for Aronia and elderberry in North America. *New York Fruit Quarterly*, 9(3), pp. 2–3.

Medina-Meza, I.G., Boioli, P. and Barbosa-Cánovas, G. V., 2016. Assessment of the effects of ultrasonics and pulsed electric fields on nutritional and rheological properties of raspberry and blueberry purees. *Food and Bioprocess Technology*, 9, pp. 520–531. https://doi.org/10.1007/s11947-015-1642-5.

Miki, J., Asanuma, M., Tachibana, Y. and Shikada, T., 1995. Novel catalyst systems for phenol synthesis by vapor phase oxidation of benzoic acid. *Bulletin of the Chemical Society of Japan*, 68(8), pp. 2429–2437. https://doi.org/10.1006/jcat.1995.1034.

Mossberg, B., Stenberg, L., Vuokko, S. and Väre, H. (eds), 2005, *Suuri Pohjolan kasvio*. Tammi, Helsinki.

Okello, A., Owuor, B. O., Namukobe, J., Okello, D. and Mwabora, J., 2022. Influence of the pH of ANCs on the efficiency of dye sensitized solar cells. *Heliyon*, 8(7):e09921. https://doi.org/10.1016/j.heliyon.2022.e09921.

Özkan, M., Dimic-Misic, K., Karakoc, A., Hashmi, S.G., Lund, P., Maloney, T. and Paltakari, J. 2016. Rheological characterization of liquid electrolytes for drop-on-demand inkjet printing. *Organic Electronics.* 38, pp. 307–315. https://doi.org/10.1016/j.orgel.2016.09.001.

Perišić, M., Barceló, E., Dimić-Mišić, K., Imani, M. and Spasojević Brkić, V., 2022. The role of bioeconomy in the future energy scenario: a state-of-the-art review. *Sustainability*, 14(1):560. https://doi.org/10.3390/su14010560.

Ridgway, C.J. and Gane, P.A.C., 2005. Ink-coating adhesion: the importance of pore size and pigment surface chemistry. J*ournal of Dispersion Science and Technology*, 25(4), pp. 469–480. https://doi.org/10.1081/DIS-200025717.

Ridgway, C. J., Schoelkopf, J. and Gane, P. A. C., 2003. A new method for measuring the liquid permeability of coated and uncoated papers and boards. *Nordic Pulp & Paper Research Journal*, 18(4), pp. 377–381. https://doi.org/10.3183/npprj-2003-18-04-p377-381.

Rousseau, J., 1945. Le folklore botanique de Caughnawaga. *Contributions de l'Institut botanique l'Universite de Montreal*, 55, pp. 7–72.

Rousseau, J., 1947. Ethnobotanique abenakise. *Archives de Folklore*, 11, pp. 145–182.

Sant'Anna, V., Gurak, P.D., Marczak, L.D. and Tessaro, I.C., 2013. Tracking bioactive compounds with colour changes in foods-A review. *Dyes and Pigments*, 98(3), pp. 601–608. https://doi.org/10.1016/j.dyepig.2013.04.011.

Sarv, V., Venskutonis, P. R., Rätsep, R., Aluvee, A., Kazernavičiūtė, R. and Bhat, R., 2021. Antioxidants characterization of the fruit, juice, and pomace of sweet rowanberry (Sorbus aucuparia l.) cultivated in Estonia. *Antioxidants*, 10(11):1779. https://doi.org/10.3390/antiox10111779.

Schön, C., Mödinger, Y., Krüger, F., Doebis, C., Pischel, I. and Bonnländer, B., 2021. A new high-quality elderberry plant extract exerts antiviral and immunomodulatory effects in vitro and ex vivo. *Food and Agricultural Immunology*, 32(1), pp. 650–662. https://doi.org/10.1080/09540105.2021.1978941.

Singh, S., Gaikwad, K. K., and Lee, Y. S., 2018. Anthocyanin – A natural dye for smart food packaging systems. *Korean Journal of Packaging Science and Technology*, 24(3), pp. 167–180. https://doi.org/10.20909/kopast.2018.24.3.167.

Skupien, K., Ochmian, I. and Grajkowski, J., 2008. Influence of mineral fertilization on selected physical features and chemical composition of aronia fruit. *Acta Agrophysica*, 11(1), pp. 213–226.

Smith, H.H., 1933. Ethnobotany of the forest potawatomi indians. *Bulletin of the Public Museum of the City of Milwaukee,* 7, pp. 1–230.

Sokolov, S.Y. (2000) Phytotherapy and phytopharmacology: a guide for doctors. *Medical news Agency*, Moscow, 976.

Taheri, R., Connolly, B. A., Brand, M. H. and Bolling, B. W., 2013. Underutilized chokeberry (Aronia melanocarpa, Aronia arbutifolia, Aronia prunifolia) accessions are rich sources of ANCs, flavonoids, hydroxycinnamic acids, and proanthocyanidins. *Journal of Agricultural and Food Chemistry*, 61(36), pp. 8581–8588. https://doi.org/10.1021/jf402449q.

Tahir, H. and Saad, M., 2021. Chapter 3 – Using dyes to evaluate the photocatalytic activity. In: M. Ghaedi, ed. *Interface Science and Technology*. 32nd ed. [online], pp. 125–224. https://doi.org/10.1016/B978-0-12-818806-4.00005-X.

Tolić, M-T., Jurčević, I., L., Krbavčić I. P., Marković, K. and Vahčić, N., 2015. Phenolic content, antioxidant capacity and quality of chokeberry (Aronia melanocarpa) products. *Food Technology and Biotechnology*, 53(2), pp. 171–179. https://doi.org/10.17113/ftb.53.02.15.3833.

Vandeput, B., 2021. *Baroa belaobara: berryapple*. PhD. Aalto University. Department of Art. *University Publication Series Doctoral Dissertations*, 65/2021. Available at: https://aaltodoc.aalto.fi/items/d210ecd3-031c-4c15-bc42-6960c21abcfb [Accessed 10 December 2024].

Vatai, T., Škerget, M., Knez, Ž., Kareth, S., Wehowski, M. and Weidner, E., 2008. Extraction and formulation of anthocyanin-concentrates from grape residues. *The Journal of Supercritical Fluids*, 45(1), pp. 32–36. https://doi.org/10.1016/j.supflu.2007.12.008.

Velmurugan, P., Vedhanayakisri, K. A., Park, Y. J., Jin, J. S. and Oh, B. T., 2019. Use of Aronia melanocarpa fruit dye combined with silver nanoparticles to dye fabrics and leather and assessment of its antibacterial potential against skin bacteria. *Fibers Polymers,* 20, pp. 302–311. https://doi.org/10.1007/s12221-019-8875-2.

Wathon, M.H., Beaumont, N., Benohoud, M., Blackburn, R.S. and Rayner, C.M., 2019. Extraction of ANCs from Aronia melanocarpa skin waste as a sustainable source of natural colorants. *Color Technology*, 135(1), pp. 5–16. https://doi.org/10.1111/cote.12385.

Woo, H.W. and Lee, J.S, 2021. Characterization of electrospun Aronia melanocarpa fruit extracts loaded polyurethane nanoweb. *Fashion and Textiles*, 8, pp. 1–4. https://doi.org/10.1186/s40691-021-00250-z.

Wu, K.T., 1997. *Acid resistant calcium carbonate filler*; ECC International Inc., WO 97/08247.

Zhang, P., Chu, F., Zhou, M., Tao, B. and Miao, F., 2024. DSSC using natural dye sensitized and Ag/CdS/TiO_2 composite structured light anode. *Vacuum*, 219:112763. https://doi.org/10.1016/j.vacuum.2023.112763.

Živković, I.P., Jurić, S., Vinceković, M., Galešić, M.A., Marijan, M., Vlahoviček-Kahlina, K., Mikac, K. M. and Lemic, D. 2020. Polyphenol-based microencapsulated extracts as novel green insecticides for sustainable management of polyphagous brown marmorated stink bug (Halyomorpha halys Stål, 1855). *Sustainability*, 12(23):10079. https://doi.org/10.3390/su122310079.

TOPICALITIES

Edited by Markéta Držková

CONTENTS

News & more

New and modified ISO standards for graphic technology

The following overview includes new and revised technical specifications and standards, developed under the direct responsibility of the technical committee ISO/TC 130 and published recently; the documents that passed the systematic review and remain current are presented in the side column.

ISO/TS 10128:2023
Graphic technology – Methods of adjustment of the colour reproduction of a printing system to match a set of characterization data

The first version of this standard from 2009 specified three methods for adjusting the digital content data to accomplish consistency in the printed results among different presses, namely using matching tone value curves based on the tone value increase (TVI), near-neutral scales, or CMYK to CMYK multi-dimensional transforms. The original edition is now replaced by this second one, which was published in November 2023 after more than two years of development. The current standard adds the fourth method for press calibration – the colour-optimised correction curve set. It also adds another measure of printed tone as an option for the first method – colour tone value (CTV), describing the apparent halftone area for colour according to ISO 20654, which defines the procedure for the measurement and calculation of spot colour tone value, see JPMTR Vol. 6, No. 3 (2017); however, in the scope of ISO/TS 10128, applicable to printing systems that use CMYK colourants, it can also be applied for process colours.

ISO 12643-1:2023, ISO 12643-2:2023, ISO 12643-3:2023, ISO 12643-4:2023 and ISO 12643-5:2023
Graphic technology – Safety requirements for graphic technology equipment and systems
Part 1: General requirements
Part 2: Prepress and press equipment and systems
Part 3: Binding and finishing equipment and systems
Part 4: Converting equipment and systems
Part 5: Manually-fed stand-alone platen presses

Since November 2023, new versions of all five parts of this standard, which harmonises requirements of the applicable U.S. and European safety standards and is relevant especially to machine manufacturers of all sizes and various health and safety bodies, are available. The first three parts, previously in the second editions from 2009 and 2010, are now in the third edition, while the last two parts, originally published in 2010, are now in the second edition.

The general requirements in the most extensive Part 1 address recognised hazards related to mechanical and electrical performance, slipping, tripping and falling, ergonomics, noise, ultraviolet and laser radiation, fire and explosion, thermal processes, substances and material used for processing, control system failure or malfunction, or emissions such as ozone, ink mist, volatile organic compounds, etc. The current edition includes revised requirements for guards, hold-to-run controls, reel unwinding and rewinding devices and

Recently reviewed and confirmed ISO standards for graphic technology

Among the standards confirmed for the first time, ISO 19593-1:2018 Graphic technology – Use of PDF to associate processing steps and content data – Part 1: Processing steps for packaging and labels, see JPMTR Vol. 7, No. 3 (2018), remains current after the review in 2023; however, the committee draft of the second edition was registered in November 2024 and the new version is now under development.

Other three recently confirmed standards were published later in 2018 and presented in JPMTR Vol. 8, No. 3 (2019); these include ISO 19302 Graphic technology – Colour conformity of printing workflows, ISO 20294 Graphic technology – Quantification and communication for calculating the carbon footprint of e-media, and ISO 21632 Graphic technology – Determination of the energy consumption of digital printing devices including transitional and related modes; the last one with Amendment 1 from 2020.

The remaining ISO documents that were first reviewed and confirmed recently comprise the standard ISO 20677:2019 Image technology colour management – Extensions to architecture, profile format, and data structure, see JPMTR Vol. 8, No. 3 (2019), and three technical specifications. The latter were all published in 2020 and presented in JPMTR Vol. 10, No. 3 (2021). Namely, they include ISO/TS 15311-1 Graphic technology – Requirements for printed matter for commercial and industrial production – Part 1: Measurement methods and reporting schema (Edition 3), ISO/TS 19303-1 Graphic technology – Guidelines for schema writers – Part 1: Packaging printing, which was confirmed in 2023 and since 2024 its revision has started, and ISO/TS 23031

Graphic technology – Assessment and validation of the performance of spectrocolorimeters and spectrodensitometers.

In the group of repeatedly reviewed and confirmed standards, the oldest one is ISO 11084-1:1993 Graphic technology – Register systems for photographic materials, foils and paper – Part 1: Three-pin systems (for the fifth time). This standard specifies the positions and dimensions for the register holes and pins and is very short. Further, all four parts of ISO 12637 Graphic technology – Vocabulary were reconfirmed in 2024. Part 1: Fundamental terms (2006), Part 2: Prepress terms (2008), and Part 4: Postpress terms (2008) were confirmed for the fourth time, while the newest one, i.e. Part 3: Printing terms from 2009, for the third time. It is also the longest part, defining almost 150 terms for printing systems and processes. When published, it also incorporated the terms and definitions from ISO 12637-5:2001 Graphic technology – Multilingual terminology of printing arts – Part 5: Screen printing terms, which was at the same time withdrawn.

Finally, the recently reviewed standards include four documents from 2013. all confirmed for the second time. These are ISO 12640-5 Graphic technology – Prepress digital data exchange – Part 5: Scene-referred standard colour image data (RIMM/SCID), two parts of ISO 12647 Graphic technology – Process control for the production of half-tone colour separations, proof and production prints, Part 1: Parameters and measurement methods and Part 3: Coldset offset lithography on newsprint, both in the third edition, and ISO 16759 Graphic technology – Quantification and communication for calculating the carbon footprint of print media products. The last one guides printers, print buyers, consumers, industry and any other interested parties in communicating and verifying carbon footprint information. It considers processes, materials and technologies required to produce print media products and allows for calculations of their whole or part life cycle.

transport systems, pile carrier movements at feeders and deliveries, and adds a new section on doctor blades, while interlocks are covered in other parts. Further, it revises the requirements for UV radiation, explosion and fire protection, and control systems. Also, it clarifies some descriptions and incorporates other changes, e.g. adapted colours, listings of the validation methods for all safeguarding measures and the noise comparison values.

The revisions made to Part 2 of ISO 12643 include definitions and requirements for large-format inkjet printing machines, new requirements for in-running nips on anilox rollers and cylinders or rollers in gravure printing presses, the movement of the inkjet heads when closing a protective device, dust protection, emergency stop devices and stop/safe pushbuttons for web offset printing presses, as well as the changes in the requirements for securing whole body access on deliveries and automatic or semi-automatic printing plate changing. In Part 3, the new requirements are related to feeders and feeding sections at gathering machines, milling head cutters and emergency stop at perfect binders, and retraction of knife and clamp at guillotine cutters. The revised requirements deal with residual pile monitoring on hopper feeders and gathering machine feeders, as well as temperature control and monitoring in the glueing unit of perfect binders and hardcover lines. The current edition of Part 4 includes the changes in the requirements for corrugated board machinery, e.g. the movable splicer module, and new requirements for the delivery of automatic flatbed die-cutting machines. Part 5 revises the requirements related to access from the front side, timer-controlled operation and stopping distance and performance, and defines new requirements for positioning laser scanners, using vision-based protective devices, and the content of the instruction handbook.

ISO 15339-1:2024
Graphic technology – Printing from digital data across multiple technologies – Part 1: Principles

This standard describes the use of colour characterisation data and their adjustment for substrate colour differences. It replaces the publicly available specification ISO/PAS 15339-1:2015, see JPMTR Vol. 4, No. 3 (2015).

ISO/TS 18621-22:2024 and ISO/TS 18621-31:2024
Graphic technology – Image quality evaluation methods for printed matter
Part 22: Evaluation of colour graininess
Part 31: Evaluation of the perceived resolution of printing systems with the Contrast–Resolution chart

The new Part 22 from May 2024 specifies test and measurement conditions and a procedure for computing the colour graininess score, S_{CG}, to quantify microscopic but visible aperiodic fluctuations of colour in the printed image. The second version of Part 31 from January 2024 replaces the 2020 edition, see JPMTR Vol. 12, No. 3 (2021); the work on the third edition is in progress.

ISO 24487:2023
Graphic technology – Processless lithographic plates – Evaluation methods for characteristics and performance

This document from December 2023 replaces ISO 24487-1:2021, see JPMTR Vol. 11, No. 3 (2020). Besides removing the part number, the new version adds definitions of plate tone value and printed tone value and three assessment methods – scratch resistance, image visibility and run length.

Bookshelf

Generative AI in Higher Education
The ChatGPT Effect

This book deals with a topic that has recently become one of the most debated across various fields and in different contexts, with education being one of the highest priorities. The authors introduce artificial intelligence (AI), track the latest developments in generative AI, explain related concepts, and address individual aspects relevant to higher education to help readers embrace the potential of generative AI in this area.

The first chapter begins with definitions of AI and its three types, Big Data and the Internet of Things. Then, it focuses on generative AI and its applications, concerns and challenges, discussing ChatGPT by OpenAI as a ground-breaking tool in education. It also illustrates the way ChatGPT works and how images are generated from text. The second chapter highlights the importance of AI literacy as an integral part of general digital literacy today, as well as its distinctions in different professional contexts. It presents existing AI literacy frameworks, introduces the dynamic model for specific roles, elaborates on the definition of AI literacy for teachers, and identifies the advantages and disadvantages of developing AI literacy.

Three chapters explore the implications of generative AI for curriculum design, assessment and education policy. Based on the published research complemented by the extensive study of opinions of both students and teachers presented in online fora or direct discussions, the authors review the identified oportunities along with the current shortcomings and risks. The list of positive features includes user-centric design, humanistic conversational style, variability, multimodal capability, scalability, customisability, comprehensive coverage, contextual relevance, multilingual support, appropriateness of topics, and code generation. Some are, at the same time, weaknesses, such as variability inherently leading to less consistent output and complicating verifications. Potential threats are also connected with a decline in critical and creative thinking, in-depth understanding, and other competencies and skills, limited social interactions, resource and technical barriers, and, last but not least, ethical concerns. Combined with the insight into designing effective prompts and ChatGPT-4's capabilities to remember, understand, apply, analyse, evaluate and create, the authors provide examples of utilising generative AI in a wide range of activities from teaching to administrative tasks. Further, the strategies enhancing the effectiveness of assessments while preserving the integrity and nine categories of the assessment types suitable for AI integration are discussed in detail, together with approaches and tools for detecting AI-generated text. Similarly, ethical principles and AI-related concerns are analysed in the context of developing AI policy, with examples implemented around the world and recommendations specific to higher education. The last two chapters are dedicated to the technology behind generative AI, the state-of-the-art models and the future of AI in education.

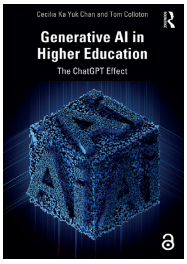

Authors: Cecilia K. Y. Chan, Tom Colloton

Publisher: Routledge
1st ed., March 2024
ISBN: 978-1-03-259904-5
286 pages, 32 images
Softcover
Available also as an eBook

Innovative Technologies for Printing, Packaging and Digital Media

Editors: Huihui Song, Min Xu, Li Yang, Linghao Zhang, Shu Yan

Publisher: Springer
1st ed., January 2024
ISBN: 978-9819999545
582 pages, 353 images
Hardcover
Also as an eBook

This volume includes a selection of over 70 peer-reviewed papers from the 14th China Academic Conference on Printing and Packaging held in Beijing in November 2023. In addition to the topics covered in previous years, from colour and image processing to printing, packaging and mechanical engineering to materials, this edition also deals with information engineering and artificial intelligent technology. The papers deal, for example, with colour measurement geometries for optically variable inks, highly precise detection of register error based on machine vision, numerically investigated spreading behaviour of inkjet droplets on rough substrates, 3D-printed micro-needle blood glucose sensor, food delivery boxes utilising phase change materials for thermal energy storage, fatigue life prediction analysis of the machete arm in web folding mechanism, electrochromic materials and devices, and intelligent package quality inspection system.

Textile Printing

Author: N. N. Mahapatra

Publisher: CRC Press
1st ed., February 2024
ISBN: 978-1032630083
204 pages
Hardcover
Also as an eBook

After the introduction, the chapters of this book discuss direct printing, roller printing, resist printing, screen printing, discharge printing, block printing, digital textile printing, transfer printing, garment printing, and yarn printing (space dyeing).

Knowledge Production Modes between Science and Applications
Volume 1: Concepts
Volume 2: Applications

The main chapters of these two volumes are preceded by extensive sections of the preface, stressing the importance of innovations as a driver of general progress, and of the introduction, elucidating the author's background in the field of 3D, 4D and bioprinting, current conditions in the academic research and industry, especially in the French context, and various aspects affecting the chances to invent and transform the invention into innovation. The first volume discusses the factors and processes towards invention and then innovation, i.e. ideas and concepts, creativity, constraints, disruptions and crises, a proof of concept, innovation models, as well as the so-called valleys of death, the role of the rational framework, interdisciplinarity, heuristics, methodologies, innovation policies, and standardisation. The second volume begins with an in-depth account of socially responsible research and then focuses on 3D, 4D and bioprinting innovations and creativity in additive manufacturing. The concluding section provides the author's vision of research and emphasises that science must acknowledge its social responsibility.

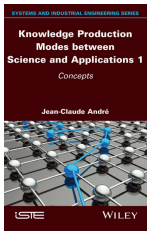

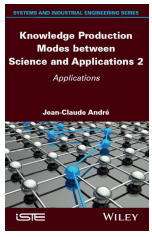

Author: Jean-Claude Andre

Publisher: Wiley-ISTE
1st ed., April & May 2024
ISBN: 978-1-786-30807-8 & 978-1-786-30935-8
288 & 272 pages
Hardcover
Available also as an eBook

Motion and Path Planning for Additive Manufacturing

This book provides background information on additive manufacturing, mechanical systems, kinematics, motion platforms, and kinematic arrangements, including robotic arm configurations with six degrees of freedom, as well as file formats for geometry data storage. Further, it describes the slicing process. It deals with cross-sectioning to define individual polygon layers and generating toolpaths for closed-loop contours of perimeters and insets, space-filling paths of infills and skins, open-loop paths (so-called skeletons), and the secondary paths providing support and assisting the process, e.g. by levelling the build plate and reducing first layer delamination. It also examines path modifiers to enhance the toolpath printability, the definition of path directions, ordering and connections, and toolpath considerations for thermoplastics, thermosets, and concrete. Further, it covers specifics of directed energy deposition processes, non-extrusion processes, off-axis and nonplanar slicing, five-axis systems with two rotary axes, and hybrid ad-

Authors: Alex C. Roschli, Michael C. Borish, Abby K. Barnes, Thomas A. Feldhausen, Peter Wang, Eric MacDonald

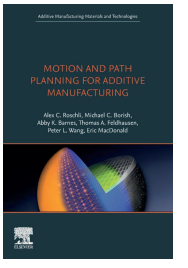

Publisher: Elsevier
1st ed., November 2023
ISBN: 978-0-443-15286-3
296 pages
Softcover
Available also as an eBook

ditive manufacturing, combining both additive and subtractive processes. Then, it explains the purpose and contents of the g-code file with the commands controlling the 3D printer. Finally, it discusses next-generation slicing approaches, such as sensor feedback, slice-on-demand capabilities, g-code streaming, support and integration of simulations, and novel visualisation and interaction modalities, e.g. using augmented reality.

The Book of Colour Concepts

These two volumes in a slipcase are dedicated to the evolution of dealing with various aspects of colour in art, science, education, industry and other contexts between the years 1686 and 1963. The content builds on carefully collected and organised archival sources, from well-known charts and works to rare or forgotten records. The first volume begins with an introductory essay from A. Loske. Its four chapters deal with early charts and tables, circles, wheels and globes, the rise of colour theory, and nomenclatures and standards. In the introduction to the second volume, S. Lowengard discusses the materiality of colour concepts. Five chapters focus on the teaching of colour, the early 20th century, spiritualism, occultism and music, Eastern colour concepts, and Bauhaus and beyond. The hundreds of quality illustrations are complemented by texts in English, French, German and Spanish.

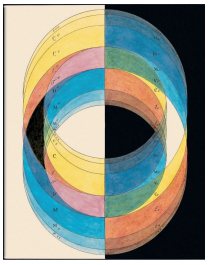

Editor: Alexandra Loske
Author: Sarah Lowengard

Publisher: Taschen
1st ed., March 2024
ISBN: 978-3-8365-9565-0
846 pages
Hardcover

A History of Books in Ancient China

To encompass Chinese book history in an accurate and comprehensive way, the study presented in this book analyses the development of ancient Chinese books in the context of changes in cultural, social, economic and political conditions in China and its regions across the vast time period of more than three thousand years, from the first inscriptions and later origins of Chinese book industry in dynasties before Confucius up to the 'New Culture Movement' in the 20th century. In eight chapters, the author describes and analyses the content, publishing, printing and collecting of books. The evolution of carriers and bindings of ancient Chinese books, from oracle bones to books with thread-stitched binding as the most mature form, is described in an appendix before the conclusion.

Author: Li Chen

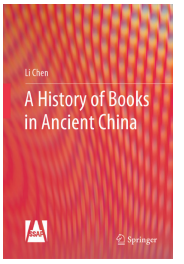

Publisher: Springer
1st ed., May 2024
ISBN: 978-981-99-8939-3
476 pages, 70 images
Hardcover
Available also as an eBook

Digital Transformation in Design Processes and Practices

Editor: Laura S. Scherling

Publisher: Transcript
1st ed., June 2024
ISBN: 978-3837671421
298 pages
Softcover
Also as an eBook

The essays in the first part of this book discuss equitable processes and practices in digital design, including the importance of trust and trustworthiness, a range of ethical considerations, digital typography and its responsiveness to devices, physical spaces and cognition, the challenge of closing the digital divide, and also the trends in technology, such as the use of non-fungible tokens, design of virtual worlds, artificial intelligence utilisation and technological transformations in textile design. The second part includes case studies and interviews exploring the relationships between digital transformation, design and education. For example, E. Lupton points out changes in design education, the problems students face today and the support they need.

The International Politics of Logos
Colours, Symbols, Cues, and Identities

Authors: Matteo C. M. Casiraghi, Eugenio Cusumano

Publisher: Routledge
1st ed., December 2023
ISBN: 978-1032500171
178 pages, 46 images
Softcover
Also as an eBook

This book presents a systematic study of over two thousand logos of different types of organisations, from political parties to private military and security companies to terrorist groups, applying qualitative and quantitative analyses of the types of logos, colours, symbols and other features they use. The study also examines their regional differences and the changes over time.

Perovskite Light Emitting Diodes
Materials and Devices

Author: Hong Meng

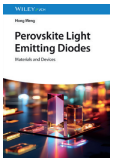

Publisher: Wiley-VCH
1st ed., January 2024
ISBN: 978-3527353200
368 pages
Hardcover
Also as an eBook

First, this book describes the structure and physical properties of metal halide perovskites, with a focus on luminescence and light-emitting diodes, and the methods and processes for their synthesis and preparation, including the use of printing. Then, it details different perovskite materials and devices emitting in near-infrared, red, green and blue spectral regions, together with specific fabrication and optimisation processes and effects of metal ion doping. It also covers lead-free metal halide perovskite materials, white light-emitting materials and devices, and electron and hole transport materials. Finally, it explores the stability of perovskite light-emitting diodes and various morphologies of perovskite lasers.

Tribological Aspects of Additive Manufacturing

Editors: Rashi Tyagi, Ranvijay Kumar, Nishant Ranjan

Publisher: CRC Press
1st ed., April 2024
ISBN: 978-1032509754
252 pages
Hardcover
Also as an eBook

This book presents the studies of the tribological behaviour of additively manufactured materials and parts and the effects of types and parameters of the 3D printing process on wear, friction, and lubrication. It covers alloys, thermoplastic polymers, polymer-matrix composites reinforced with metal powder, carbon fibres or various natural fibres, tribocorrosion properties of orthopaedic implants, emerging applications of 3D-printed parts with enhanced tribological properties, and other applications.

Stimuli-responsive Actuating Materials for Micro-robotics

The authors present the stimuli-responsive materials and their use in micro-robotic devices as a solution closing the gap between conventional motors and actuators and nanorobots powered by molecular motors. The book describes piezoelectric ceramics, shape memory alloys, nanoporous metals, both electroactive and non-electroactive polymer actuators, polymer gels, carbon nanotubes, and graphene-based actuators. Also, it deals with novel actuating material types, including those based on transitional metal oxides and hydroxides, as well as carbides and nitrides (i.e. 2D materials called MXenes), and 2D MoS_2. Further, it discusses multi-material systems, such as hydraulically amplified self-healing electrostatic actuators, and additional robotic functions, e.g. compact actuation and sensing or energy generation, enabled by multi-stimuli-multi-response materials. One chapter describes the enabling technologies – fabrication processes, including 3D and 4D printing, special techniques for enhancing robotic functions, and chemo-mechanics analysis of actuators. Another one is dedicated to applications, namely bionic robotic fish and jellyfish, swimming robots, flying robots, terrestrial robots, delta and gripper robots, soft grippers, and surgical devices. The book concludes with a comparison of actuating materials and an outlook on future development.

Authors: Kenneth K. W. Kwan, Alfonso H. W. Ngan

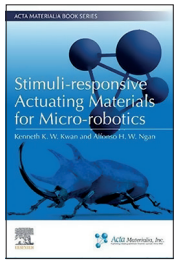

Publisher: Elsevier
1st ed., February 2024
ISBN: 978-0-443-16094-3
302 pages
Softcover
Available also as an eBook

Smart and Connected Wearable Electronics
Nanomanufacturing, Soft Packaging, and Healthcare Devices

The main content of this book, with almost 40 contributors, is organised into three parts. The first one deals with printing-enabled nanomanufacturing of sensors and electronics, with the chapters focused on screen printing, inkjet printing, aerosol jet printing and roll-to-roll printing. The second part describes soft material packaging for hybrid flexible bioelectronics. It details integration strategies, fabrication methods and materials, from substrates to interconnections to encapsulation, as well as materials and technologies suitable for human–machine interfaces. The applications of wearable electronics for healthcare devices, presented in the third part, include devices monitoring electrophysiological signals and gaseous biomarkers, implantable soft electronics and sensors, and powering technologies.

Editors: Woon-Hong Yeo, Yun Soung Kim

Publisher: Woodhead Publishing
1st ed., November 2023
ISBN: 978-0-323-99147-6
588 pages
Softcover
Available also as an eBook

Bookshelf

Academic dissertations

Chemical and Particulate Contaminants Produced in Additive Manufacturing (3D Printing) of Plastics

Doctoral thesis – Summary

Author:
Antti Väisänen

Speciality field:
Environmental Science

Supervisors:
Marko Hyttinen
Pertti Pasanen

Defended:
27 January 2023,
University of Eastern Finland, Faculty of Science, Forestry and Technology, Department of Environmental and Biological Sciences
Kuopio, Finland

Contact:
antti.vaisanen@uef.fi

This thesis contributes to the research on additive manufacturing safety, which continues to gain importance with the significant growth in the use of both industrial and consumer-scale machines, while the associated occupational and operational hazards are not sufficiently explored and identified. Exposure to various contaminants can arise during all stages of the production process and also later during product use. This work is focused on gaseous or particulate air pollutants in polymer additive manufacturing. The aim was to document the exposure levels of identified agents and compare the obtained data with the known threshold values as well as among the individual additive manufacturing methods studied.

The dissertation provides the background on relevant additive manufacturing methods, including material extrusion, vat photopolymerisation, powder bed and multi-jet fusion and material jetting, along with the corresponding polymer materials, i.e. thermoplastic filaments and pellets, photocurable resins, powders and composites, as well as the monitored categories of indoor air pollutants, namely volatile organic compounds and particles classified as dust or coarse, fine and ultrafine. The review chapter concludes with the findings from the literature on 3D printer emissions for the methods of interest and essential exposure influencing factors. Two chapters detail the aims of the thesis and experimental methods used for sampling and analysis. The results show that the operation of all used 3D printers and feedstocks increases chemical or ultrafine particle concentrations, usually both. The values are mostly below the defined hazardous levels; however, for many detected compounds, the limits are not available. The results for sustainable and generic feedstocks were similar. Coarse particles exceeded the limits when handling powdered feedstocks in the pre- and post-processing stages. Similarly, post-production material outgassing was identified as a potential risk if products were not correctly post-processed and stored.

Further reading:
ISBN: 978-952-61-4769-7

3D Printed Piezoelectric Energy Harvesters

Doctoral thesis – Summary

Author:
Xinran Zhou

Speciality field:
Materials Science and Engineering

Supervisor:
Lee Pooi See

Defended:
2 May 2023, Nanyang Technological University, School of Materials Science and Engineering
Singapore

This thesis explored the 3D printing of piezoelectric materials to provide a sustainable and highly stretchable energy source for wearable electronic systems. In particular, the approach was based on formulating the piezoelectric inks and combining two 3D printing techniques, digital light projection and direct writing, to fabricate the mechanical energy harvester comprising the composite piezoelectric material and electrodes. The design was further improved by implementing a kirigami and auxetic structures. The latter enabled the device to be used as a bending angle sensor thanks to the increased bending output voltage.

The text briefly reviews the principles of energy harvesting with a focus on harvesters based on piezoelectric effect, common types of piezoelectric materials, considerations for their 3D printing and fabricating stretchable piezoelectric energy harvester, including the benefits of kirigami patterns and various auxetic structures. One chapter provides the experimental details

Contact:
zhouxr@dhu.edu.cn

regarding the selection of materials, preparation of inks and methods for fabrication of piezoelectric materials and electrodes. It also describes the methods used for the characterisation of materials and samples, together with simulations using the finite element method. Three chapters present the individual types of energy harvesters. First, the all-3D-printed stretchable piezoelectric nanogenerator was fabricated using ink with piezoelectric ceramic barium titanate nanoparticles and photocurable acrylate oligomers. The output voltage was improved by printing a staggered strip structure. The resulting sensor showed stretchability over 400 % and a large sensing range but low sensitivity; its performance was stable up to 100 % tensile strain. Second, the piezoelectric nanoparticles were incorporated in the poly(vinylidenefluoride-co-trifluoroethylene) matrix. The modified kirigami structure with a T-joint cut allowed the fabrication of the device to be suitable for wearable applications, including gait sensing, with strain up to 300 % without degradation in output voltage. Finally, the barium titanate nanoparticles were surface-modified to enhance piezoelectricity, ferroelectricity and dielectric constant of the composite. The additional 3D-printed auxetic structure enabled the generation of energy not only by pressing and stretching but also by bending.

Further reading:
DOI: 10.32657/10356/166595

Doctoral thesis – Summary

Author:
Felix Braig

Speciality field:
Mechanical Engineering

Supervisors:
Edgar Dörsam
Tatiana Gambaryan-Roisman

Defended:
20 December 2023, Technical University of Darmstadt, Department of Mechanical Engineering, Institute of Printing Science and Technology Darmstadt, Germany

Language:
German

Original title:
Untersuchung der Lösungsmittelatmosphäre von verdunstenden, gedruckten Fluidfilmen mittels digitaler, holographischer Interferometrie

Contact:
felix.braig@googlemail.com

Investigation of the Solvent Atmosphere of Evaporating Printed Liquid Films Using Digital Holographic Interferometry

The research within this thesis was concerned with the field of drying thin liquid films with a focus on the evaporation process and the possible ways of improving it. This knowledge can help to achieve higher homogeneity of printed layers, among other application areas. The approach was based on studying the spatial distribution of the solvent vapour in close proximity to the film surface, which reflects the local evaporation rates. Their differences lead to concentration gradients in the fluid film that can result in flows within the printed layer and, consequently, defects and other non-uniformities in the dried layer. The work employed the analysis of images acquired by an interferometric system. A six-axis robot and an inkjet printing system were used to ensure the required precision in the printing and manipulation of samples.

The dissertation introduces the basics of the inkjet printing process and the theoretical background on the evaporation of solvents, with the considerations of free enthalpy and saturation vapour pressure for pure fluids and binary liquid mixtures. Further, it covers mass transport in gases, including convective mass and heat transport and the fluid dynamic boundary layer theory, the numerical simulations used in the experimental design, the Fourier transform and its application to two-dimensional image data, and an overview of recent publications in the considered domain. The experimental details include the measurement concept, called digital holographic interferometry and based on changes in the refractive index of air above the evaporating film of ethylene glycol with ethanol, the setup comprising a Michelson interferometer, an inkjet printing unit and a robotic platform, the characterisation of the camera sensor, an experimental plan and the image analysis method, including the analysis of the reference images and interferograms, phase unwrapping, the concentration distribution calculations, and their limitations. Finally, the dissertation presents the spatial distribution and temporal evolution of ethanol vapour molar concentrations, allowing conclusions to be drawn about the vapour flow above the thin liquid film. It discusses the influences of the substrate inclination during evaporation and the width of the printed film, as well as the diffusion flux near the phase interface, temperature effects, and the evaluation at low solvent concentrations.

Further reading:
DOI: 10.26083/tuprints-00026632

Events

Textile Printing & Sustainability Conference 2024

Düsseldorf-Neuss, Germany
15–16 October 2024

In its second edition, the programme of this ESMA event begins with two keynotes focused on the EU's Ecodesign for Sustainable Products Regulation (ESPR) and Digital Product Passport (DPP) requirements, as well as the role of safe chemicals, essential to the sustainability performance. The next two keynotes deal with polysaccharide-based screen-printing inks and the current challenges in education and training in the textile printing sector. On the second day, the keynotes cover the trends towards the circular digital textile and surface decoration industry, the progress in direct-to-film technology, the impact of fast or slow fashion on garment quality, the key principles of circularity, and the strategies supporting the environmentally responsible approach. Sustainability and digital transformation are also reflected in other contributions, together with new materials, hardware and software solutions and innovative processes.

American Printing History Association Annual Conference 2024

New York City, New York & Berkeley, California, USA
17–19 October 2024

The association celebrates its 50th anniversary with a special hybrid conference that combines two locations and virtual as well as in-person events, including a workshop, tours and presentation sessions. Among the keynotes, the intriguing topic, encompassing the printing history, specimen books and generative artificial intelligence struggling with text, is presented by Lisa Gitelman in her talk entitled 'Typographic hallucination, or, a conversation imagined between artificial intelligence and the printing trades'.

GRID 2024
12th International Symposium on Graphic Engineering and Design

Novi Sad, Serbia
14–16 November 2024

This edition features three plenary speakers. The keynotes of the first two focus on packaging – the topics are sustainable packaging solutions by Urška Vrabič Brodnjak and current trends in packaging by Emine Arman Kandirmaz. The title of the third keynote by Charles T. Weiss is 'Transforming the classroom with design thinking'. The following sessions are organised into two tracks, complemented by the industry session on the second day. On the last day, the symposium concludes with a round-table discussion. The numerous posters mostly deal with printing quality, digital media, novel technologies and artificial intelligence. In addition, they cover the topics of education, typography, design, packaging added value, ecology, paper as a substrate, and print finishing.

User Forum UV Printing 2024

Aschheim, Germany
5–6 November 2024

This event is held every two years, only in German. With the 2024 slogan 'LED the future start!', the 13th edition presents various radiation curing applications, from offset lithography and inkjet printing to metal decorating and 3D screen printing. The topics also cover differences in curing technologies, including electron-beam curing and initiator-free UV curing, environmental aspects, such as deinkability and food contact safety, materials, and more.

ICGIP 2024
16th International Conference on Graphics and Image Processing

Nanjing, China
8–10 November 2024

The programme of this established event includes, for example, a keynote by Mingyi He on 'Integrated image and graphic intelligent processing via hyperspectral multi-viewing' and papers presenting the improved handwriting recognition, calligraphic guideline generation, matching and fusion of visible and infrared images, 3D texture generation, a text-to-image customisation method for image generation, and enhanced reversible data hiding in encrypted images.

XIX Color Conference

https://www.gruppodelcolore.org
28–29 November 2024

The 2024 edition of this conference is in online format. The invited speakers are Phil Green, presenting a test chart for seven-colour printing, Vien Cheung, discussing colour association, and Robin Kingsburgh, sharing her experience in teaching a multidisciplinary course about colour.

34th International Publishers Congress

Guadalajara, Mexico
3–6 December 2024

The programme of this edition includes panel discussions on how copyright promotes freedom of expression, the opt-out mechanism for rights holders to restrict the use of their work for text and data mining, the role of trustworthy publishing in the age of fake news and deepfakes, and more.

The 2025 C!print Shows

In 2025, these shows dedicated to visual communication, printing, and personalisation take place in both locations: first in Madrid, Spain (14–16 January) and three weeks later in Lyon, France (4–6 February).

GWG Technical Meetings in 2025

The first technical meeting of the Ghent Workgroup in 2025 takes place on 22–23 January in Lisbon, Portugal, and is preceded by the educational day at ISEC Lisboa, the Higher Institute of Education and Sciences, on 21 January. The second educational day is announced for 13 May at Artevelde University of Applied Sciences in Ghent before the meeting in Merelbeke, Belgium (14–15 May). The third meeting is scheduled for 15–16 October in Orlando, Florida, USA.

Convertech 2025

Tokyo, Japan
29–31 January 2025

This converting technology exhibition is organised jointly with those showcasing new value-generating functional materials, environmentally friendly materials and equipment, and decoration technologies.

SPIE Photonics West 2025

San Francisco, California, USA
25–30 January 2025

This large event features over a hundred conferences with about five thousand presentations, comprising plenary and invited talks, technical papers, and posters; also, it offers tens of courses, industry demonstrations, and other learning or networking opportunities. The dozens of contributions that present various applications of printing are part of the programme of several conferences. The papers deal, for example, with a unique volumetric 3D printing technology for producing isotropic objects with optical-grade surfaces and other advances in volumetric 3D printing, 4D microprinting of programmable liquid crystal microstructures, 3D laser printing below the diffraction limit, optimising projection multi-photon 3D printing using convolutional neural networks, miniaturisable printed microfluidics employing the chemiluminescent reaction, as well as with novel materials and studies of physical and chemical processes underlying further development. The conference is accompanied by three exhibitions. In addition, Photonics West is co-located with the event dedicated to augmented, virtual and mixed reality, SPIE AR | VR | MR 2025, and SPIE Global Business Forum 2025, providing the market data and trends impacting the global photonics industry.

Electronic Imaging 2025

Burlingame, California USA
2–6 February 2025

For its current edition, this IS&T symposium joins 17 conferences that cover topics from human perception and cognition to media security and high-performance imaging. The announced keynotes are 'Transparency and scission in augmented reality' by Michael J. Murdoch, 'Experiencing art – changing the world to the better' by Claus-Christian Carbon, 'Predicting visible differences in virtual and augmented reality' by Alexandre Chapiro, 'Beyond the screen plane: stereo at Walt Disney Animation Studios' by Katie Fico, and the last by Daniel J. Sandin, reviewing five decades of innovation in interactive electronic displays for art and science at two U.S. universities. Of the 18 short courses, half are new, such as the one that teaches the use of Unity for perceptual and behavioural experiments in virtual reality.

innoLAE 2025
Innovations in Large-Area Electronics

Cambridge, UK
17–20 Febuary 2025

In its 11th year, this event begins with five short courses scheduled for the first two days. The programme of the following conference offers presentation sessions in two tracks, including several invited talks, and three plenary keynotes: 'On-chip learning with organic neuromorphic and biohybrid systems' by Yoeri van de Burgt, 'Lowering the barrier to entry for flexible foundry technology' by David Verity and 'Manufacturing organic semiconductors enabling high performance large area organic photovoltaics' by François Grenier.

Journal of Print and Media Technology Research
A PEER-REVIEWED QUARTERLY

ISSN 2414-6250 (Online)
ISSN 2223-8905 (Print)
UDC 665

Call for papers

The Journal of Print and Media Technology Research is a peer-reviewed periodical, published quarterly by iarigai, the International Association of Research Organizations for the Information, Media and Graphic Arts Industries.

JPMTR is listed in Emerging Sources Citation Index, Scopus, DOAJ – Directory of Open Access Journals, Index Copernicus International, NSD – Norwegian Register for Scientific Journals, Series and Publishers.

Authors are invited to prepare and submit complete, previously unpublished and original works, which are not under review in any other journals and/or conferences.

The journal will consider for publication papers on fundamental and applied aspects of at least, but not limited to, the following topics:

Printing technology and related processes
Conventional and special printing; Packaging; Fuel cells, batteries, sensors and other printed functionality; Printing on biomaterials; Textile and fabric printing; Printed decorations; 3D printing; Material science; Process control

Premedia technology and processes
Colour reproduction and colour management; Image and reproduction quality; Image carriers (physical and virtual); Workflow and management

Emerging media and future trends
Media industry developments; Developing media communications value systems; Online and mobile media development; Cross-media publishing

Social impact
Environmental issues and sustainability; Consumer perception and media use; Social trends and their impact on media

Submissions for the journal are accepted at any time. If meeting the general criteria and ethic standards of scientific publishing, they will be rapidly forwarded to peer-review by experts of relevant scientific competence, carefully evaluated, selected and edited. Once accepted and edited, the papers will be published as soon as possible.

There is no entry or publishing fee for authors. Authors of accepted contributions will be asked to sign a Licensing agreement (CC-BY-NC 4.0).

Authors are asked to strictly follow the guidelines for preparation of a paper (see the abbreviated version on inside back cover of the journal).

Complete guidelines can be downloaded from: <http://iarigai.com/publications/journals/guidelines-for-authors/>
Papers not complying with the guidelines will be returned to authors for revision.

Submissions and queries should be directed to: journal@iarigai.org

Journal of Print and Media Technology Research
A PEER-REVIEWED QUARTERLY

Vol. 13, 2024
Prices and subscriptions

Since 2016, the journal is published in digital form; current and archive issues are available at: <https://iarigai.com/publications/journals/>.

Since 2020, the journal is published as "open access" publication, available free of charge for iarigai members, subscribers, authors, contributors and all other interested public users.

A print version is available on-demand. Please, find below the prices charged for the printed Journal, for four issues per year as well as for a single issue

Regular prices

Four issues, print JPMTR (on-demand)	400 EUR
Single issue, print JPMTR (on-demand)	100 EUR

Subscription prices

Annual subscription, four issues, print JPMTR (on-demand)	400 EUR

Prices for iarigai members

Four issues, print JPMTR (on-demand)	400 EUR
Single issue, print JPMTR (on-demand)	100 EUR

Place your order online at: <http://www.iarigai.org/publications/subscriptions-orders/>
Or send an e-mail order to: office@iarigai.org

Guidelines for authors

Authors are encouraged to submit complete, original and previously unpublished scientific or technical research works, which are not under reviews in any other journals and/or conferences. Significantly expanded and updated versions of conference presentations may also be considered for publication. In addition, the Journal will publish reviews as well as opinions and reflections in a special section.

Submissions for the journal are accepted at any time. If meeting the general criteria and ethical standards of the scientific publication, they will be rapidly forwarded to peer-review by experts of high scientific competence, carefully evaluated, and considered for selection. Once accepted by the Editorial Board, the papers will be edited and published as soon as possible.

When preparing a manuscript for JPMTR, please strictly comply with the journal guidelines. The Editorial Board retains the right to reject without comment or explanation manuscripts that are not prepared in accordance with these guidelines and/or if the appropriate level required for scientific publishing cannot be attained.

A – General

The text should be cohesive, logically organized, and thus easy to follow by someone with common knowledge in the field. Do not include information that is not relevant to your research question(s) stated in the introduction.

Only contributions submitted in English will be considered for publication. If English is not your native language, please arrange for the text to be reviewed by a technical editor with skills in English and scientific communications. Maintain a consistent style with regard to spelling (either UK or US English, but never both), punctuation, nomenclature, symbols etc. Make sure that you are using proper English scientific terms. Literal translations are often wrong. Terms that do not have a commonly known English translation should be explicitly defined in the manuscript. Acronyms and abbreviations used must also be explicitly defined. Generally, sentences should not be very long and their structure should be relatively simple, with the subject located close to its verb. Do not overuse passive constructions.

Do not copy substantial parts of your previous publications and do not submit the same manuscript to more than one journal at a time. Clearly distinguish your original results and ideas from those of other authors and from your earlier publications – provide citations whenever relevant.

For more details on ethics in scientific publication consult Guidelines, published by the Committee on Publication Ethics (COPE):
<https://publicationethics.org/resources/guidelines>

If it is necessary to use an illustration, diagram, etc. from an earlier publication, it is the author's responsibility to ensure that permission to reproduce such an illustration, diagram, etc. is obtained from the copyright holder. If a figure is copied, adapted or redrawn, the original source must be acknowledged.

Submitting the contribution to the Journal, the author(s) confirm that it has not been published previously, that it is not under consideration for publication elsewhere and – once accepted and published – it will be disseminated and make available to the public in accordance to the Creative Commons Attribution-NonCommercial 4.0 International Public License (CC-BY-NC 4.0), in English or in any other language. The publisher retains the right to publish the paper online and in print form, and to distribute and market the Journal containing the respective paper without any limitations.

B – Structure of the manuscript

Preliminary

Title: Should be concise and unambiguous, and must reflect the contents of the article. Information given in the title does not need to be repeated in the abstract (as they are always published jointly), although some overlap is unavoidable.

List of authors: I.e. all persons who contributed substantially to study planning, experimental work, data collection or interpretation of results and wrote or critically revised the manuscript and approved its final version. Enter full names (first and last), followed by the present address, as well as the E-mail addresses. Separately enter complete details of the corresponding author – full mailing address, telephone number, and E-mail. Editors will communicate only with the corresponding author.

Abstract: Should not exceed 500 words. Briefly explain why you conducted the research (background), what question(s) you answer (objectives), how you performed the research (methods), what you found (results: major data, relationships), and your interpretation and main consequences of your findings (discussion, conclusions). The abstract must reflect the content of the article, including all keywords, as for most readers it will be the major source of information about your research. Make sure that all the information given in the abstract also appears in the main body of the article.

Keywords: Include three to five relevant scientific terms that are not mentioned in the title. Keep the keywords specific. Avoid more general and/or descriptive terms, unless your research has strong interdisciplinary significance.

Scientific content

Introduction and background: Explain why it was necessary to carry out the research and the specific research question(s) you will answer. Start from more general issues and gradually focus on your research question(s). Describe relevant earlier research in the area and how your work is related to this.

Methods: Describe in detail how the research was carried out (e.g. study area, data collection, criteria, origin of analyzed material, sample size, number of measurements, equipment, data analysis, statistical methods and software used). All factors that could have affected the results need to be considered. Make sure that you comply with the ethical standards, with respect to the environmental protection, other authors and their published works, etc.

Results: Present the new results of your research (previously published data should not be included in this section). All tables and figures must be mentioned in the main body of the article, in the order in which they appear. Make sure that the statistical analysis is appropriate. Do not fabricate or distort any data, and do not exclude any important data; similarly, do not manipulate images to make a false impression on readers.

Discussion: Answer your research questions (stated at the end of the introduction) and compare your new results with published data, as objectively as possible. Discuss their limitations and highlight your main findings. At the end of Discussion or in a separate section, emphasize your major conclusions, pointing out scientific contribution and the practical significance of your study.

Conclusions: The main conclusions emerging from the study should be briefly presented or listed in this section, with the reference to the aims of the research and/or questions mentioned in the Introduction and elaborated in the Discussion.

Note: Some papers might require different structure of the scientific content. In such cases, however, it is necessary to clearly name and mark the appropriate sections, or to consult the editors. Sections from Introduction until the end of Conclusions must be numbered. Number the section titles consecutively as 1., 2., 3., ... while subsections should be hierarchically numbered as 2.1, 2.3, 3.4 etc. Only Arabic numerals will be accepted.

Acknowledgments: Place any acknowledgements at the end of your manuscript, after conclusions and before the list of literature references.

References: The list of sources referred to in the text should be collected in alphabetical order on at the end of the paper. Make sure that you have provided sources for all important information extracted from other publications. References should be given only to documents which any reader can reasonably be expected to be able to find in the open literature or on the web, and the reference should be complete, so that it is possible for the reader to locate the source without difficulty. The number of cited works should not be excessive – do not give many similar examples.

Responsibility for the accuracy of bibliographic citations lies entirely with the authors. Please use exclusively the Harvard Referencing System. For more information consult the fifth edition of the Guide to Referencing in the Harvard Style, used with consent of Anglia Ruskin University, released by ARU University Library, available at:
<https://library.aru.ac.uk/referencing/harvard.htm>

C – Technical requirements for text processing

For technical requirement related to your submission, i.e. page layout, formatting of the text, as well of graphic objects (images, charts, tables etc.) please see detailed instructions at:
<http://iarigai.com/publications/journals/guidelines-for-authors/>

D – Submission of the paper and further procedure

Before sending your paper, check once again that it corresponds to the requirements explicated above, with special regard to the ethical issues, structure of the paper as well as formatting.

Once completed, send your paper as an attachment to:
journal@iarigai.org

If necessary, compress the file before sending it. You will be acknowledged on the receipt within 48 hours, along with the code under which your submission will be processed.

The editors will check the manuscript and inform you whether it has to be updated regarding the structure and formatting. The corrected manuscript is expected within 15 days.

Your paper will be forwarded for anonymous evaluation by two experts of international reputation in your specific field. Their comments and remarks will be in due time disclosed to the author(s), with the request for changes, explanations or corrections (if any) as demanded by the referees.

After the updated version is approved by the reviewers, the Editorial Board will decide on the publishing of the paper. However, the Board retains the right to ask for a third independent opinion, or to definitely reject the contribution.

Printing and publishing of papers, once accepted by the Editorial Board, will be carried out at the earliest possible convenience.

3-2024

Journal of Print and Media Technology Research

A PEER-REVIEWED QUARTERLY

The journal is publishing contributions in the following fields of research

- Printing technology and related processes
- Premedia technology and processes
- Emerging media and future trends
- Social impacts

For details see the Mission statement inside

JPMTR is listed in

- Emerging Sources Citation Index
- Scopus
- DOAJ – Directory of Open Access Journals
- Index Copernicus International
- NSD – Norwegian Register for Scientific Journals, Series and Publishers

Submissions and inquiries

journal@iarigai.org

Subscriptions

office@iarigai.org

More information at

www.iarigai.org/publications/journal

Publisher

The International Association of Research Organizations
for the Information, Media and Graphic Arts Industries
Magdalenenstrasse 2
D-64288 Darmstadt
Germany